TELECOMMUNICATION
ENGINEERING

University of Twente
The Netherlands

University of Twente
Department of Electrical Engineering
Chair for Telecommunication Engineering

Realization and characterization of a 2.4 GHz radio system based on Frequency Offset Division Multiple Access.

by

Wietse Balkema

Master thesis
Executed from December 2003 to August 2004

Supervisors: prof. dr. ir. J.C. Haartsen
prof. ir. J.L.Tauritz
Advisors: dr. Y.Shen

Abstract

The ultra-wideband communication systems that appear on the market at this moment are based on transmitting streams of extremely short pulses. A problem with this technique is synchronization of the receiver.

In the Telecommunication Engineering group of the University of Twente a lot of research has been done on the coherence multiplexing technique for the optical domain. The coherence multiplexing technique can also be used in the RF domain. Two techniques have been developed: Time offset division multiple access (TODMA) and Frequency offset division multiple access (FODMA).

In this report, results of extensive simulations in a microwave simulation program are presented. The simulations show the behavior as predicted by theory. A testbed has been built and the performance of this testbed is thoroughly examined. As a consequence of signal losses and leakage in components, there is a discrepancy between the predictions from simulations and practical measurements. Apart from this discrepancy, the system shows the expected behavior.

Contents

Chapter 1

Introduction

Over the last few years, mobile communication systems have entered into our daily lives. The demand for ad-hoc and personal area networks will be increasing. Bluetooth was a good first step in these networks, but consumers will soon need higher capacities. Companies are already advertising with their 'no wires needed' products, new methods are being developed to provide the necessary capacity.

1.1 Ultra-wideband communication systems

Currently, ultra-wideband communications is a hot-topic in communication engineering. The bandwidth of ultra-wideband systems is extremely large, at least 500 MHz. The fractional bandwidth η is at least 0.20, where η is defined as:

$$\eta = \frac{f_u - f_l}{f_u + f_l} \tag{1.1}$$

f_u and f_l are the upper and lower -3dB bandwidth edges. By spreading a data signal over a wide frequency range, high datarates can be obtained and that is what consumers will need.

At this moment, standards for ultra-wideband communications are being developed. Since we want to apply UWB in ad-hoc or personal area networks, synchronization has to be fast and efficient. The majority of the proposed systems are based on transmitting low-power streams of extremely short pulses (10 - 1000 picoseconds). A problem with these extremely short pulses is synchronization at the receiver's side. Nevertheless, the first systems using these ultrashort pulses are already on the market, and can obtain datarates of up to 114 Mbps.

All over the world, research has been done on systems that use continuous signals in place of ultrashort pulses. These systems use a chaotic, ultra-wideband signal as a spreading sequence for the data. As far as could be checked, these systems have not yet been implemented.

In December 2000 Kolumbán [1] presented three ways for transmitting data with an ultra-wideband spreading signal: *Coherent Antipodal CSK*, *Coherent DCSK* and *Differentially coherent DCSK*, where CSK stands for Chaos Shift Keying. The first two methods described assume that the spreading signal is known in the receiver. Here, synchronization is still a huge problem. In the third system, a fixed sequence is used to encode each bit. First, the coded bit is transmitted, then the unmodulated data sequence. This system has the advantage that the spreading sequence does not have to be available at the receiver, the data sequence can be obtained by correlating the received signal with a time-delayed version of the signal.

A disadvantage of the systems mentioned above is that, under the assumption that the spreading sequence is unknown at the receiver, two bit-times are used to transmit one bit: one for the actual bit transmission and one for the spreading sequence.

At the Telecommunication Engineering (TE) group at the University of Twente, a lot of research has been done on coherence multiplexing in the optical domain [2]. Coherence multiplexing systems use a broadband noise signal as a carrier for transmitting data. Together with the 'clean' noise signal, a modulated version of the noise with a small time-offset is transmitted. By correlating these two signals, the original datasequence can be retrieved. Using this technique, the spreading sequence is not transmitted *separately* from the modulated version, but it is transmitted *simultaneously*.

Recently this technique has also been applied in the microwave domain by Bekkaoui [3] and Taban [4], and is called Time Offset Division Multiple Access (TODMA). Bekkaoui determined the theoretical performance of this system and Taban succeeded in implementing a testbed for proof-of-concept measurements.

1.2 Frequency Offset Division Multiple Access

A counterpart of TODMA is the subject of this thesis project. Frequency Offset Division Multiple Access (FODMA) does not use a time offset to separate the modulated and unmodulated spreading sequence. Instead it uses an offset in the frequency domain. This concept has been the subject of investigation at the TE group. Shang [5] analyzed the theoretical performance of this system. This performance analysis is the startingpoint for the work presented in this report: the realization of a FODMA testbed.

Thusfar no systems like FODMA have been realized. Practical problems are as yet to be identified. By building a testbed, the strengths and weaknesses will become apparent and these can later on be the subject of further investigation. The project will include the following steps:

- Simulation of the system using a microwave component simulator.
- Realization of the system using standard microwave components.
- Characterization of the system in the presence of noise and jamming.
- Verification of the theory.

The outcome of this project will be the starting point for further research at the TE group.

1.3 Organization of the report

In chapter two, a short introduction to wireless communications is given. After the most relevant issues have been discussed, the FODMA system is presented. The chapter ends with a performance analysis of FODMA, based on the theoretical work of Shang.

Chapter three deals with the simulation of FODMA using Agilent EEsof's microwave simulation program *Advanced Design System*. Several simulation models are presented and the simulation results compared with the theoretical results.

In the fourth chapter an introduction to RF system design is given. Concepts of noise in cascaded systems and distortion in nonlinear elements are presented. The operation of the basic components in RF systems is explained.

Chapter five is all about the realization of and measurements using the FODMA testbed. The block schematic which is presented in chapter two is developed into a schematic with practical components. The most important properties of the components are discussed. Finally, measurement results are presented.

In chapter six conclusions will be drawn from both measurements as well as simulations. After the conclusions, some recommendations for further research will be given.

Chapter 2

Radio Theory

2.1 Introduction

In this chapter the most important theory for wireless communication systems will be presented. After a short introduction to communications history, attention will be paid to wireless transmission through the ether. In the last section the FODMA system will be presented.

2.2 History

Long-distance communications

One of the earliest methods of long-distance communications was used by the Greeks after their victory over the Trojans: they lit a chain of huge fires to let the people in Athens know about their victory. Since the amount of information carried by an ordinary fire is very small, people started developing other methods for long-distance communication. A well-known method was used by the Indians around the 16^{th} century, they sent messages over longer distances using smoke signals.

In 1792 a mechanical semaphore signaler was built in France. With this system, communication became possible between Paris an Lille in 1794. A distance of 240 kilometer was covered by 15 towers. Under good weather conditions a sign could be sent across that distance in 5 minutes (2880 km/h!).

After Faraday showed how electricity could be mechanically produced in 1831, people started investigating ways of sending messages over long distances using copper cables. Not much later, Cooke and Wheatstone realized a telegraph system for the London railway line. This system used two batteries and a switch for polar signaling. When Edison introduced his repeater telegraph, long-distance auto-relay communications became common business. It was found that fast changes in voltage on the line could be heard with a small headphone. With this principle, Bell developed the telephone in 1876.

Wireless communications

Around 1895 Popoff developed one of the first wireless communication systems for the Russian Navy. He installed a receiver that operated an electric bell in St. Petersburg which he could control at a distance of 5 kilometers. Parallel to this development, Marconi built a system which could do the same. In 1896 he took it to England for demonstration to the British Post. One year later he acquired patents for his apparatus that gave him the monopoly on wireless telegraph systems for years to come.

In 1900 Fessenden was the first to send voice messages via radio waves. One year later he demonstrated an improved version of his system in Washington, where he transmitted speech over a distance of twenty-five miles. In 1908, De Forest was the one with the first 'radio station'. He installed a transmitter at the top of the Eiffel Tower from which he broadcast music from a gramophone. Due to a lack of people who could receive it, it did not become as popular as radio was bound to become.

In the next decades, AM and later FM radio were developed. Radio became the way to remain informed about what was going on in the world. Due to the introduction of the television, radio is not the only available medium anymore but it still is an important communication medium.

In the late sixties the cellular concept was developed at Bell Labs. This concept was to be used in 1981 for the first generation of cellular phones. In the second generation (GSM), cells became smaller in order to offer huge capacities at crowded places. Decreasing cell size continues to be good practice, while the use of wireless local and municipal area networks is gaining interest.

2.3 Air as a transmission medium

The key issue to any form of communication is the received signal power and the signal to noise ratio (*SNR*). For most digital applications, a minimum Bit Error Rate (*BER*) can be defined. This BER is dependent on the received signal power and the SNR. The maximum allowed signal loss can be found from Figure 2.1. In this figure we have:

$\mathbf{P}_t$: Permitted transmit power

P_r : Required receive power

N : Noise floor

NF : Noise figure

SNR : Required SNR

FM : Fading Margin

PL : Path loss

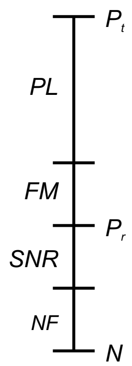

Figure 2.1: Link budget [dB]

In order to understand all the items in the figure we need to know a little bit more about air as a transmission medium for radio waves. The items of interest are the *Path Loss* and the *Fading Margin*. The path loss includes all the losses in the path from transmitter to receiver. The fading margin is the difference between required receive power and average receive power. The noise factor stands for the amount of noise added in the receiver. In the following paragraphs a short introduction to factors influencing the actual path loss is given.

2.3.1 Received signal power

In an ideal case, the transmitting and receiving antenna's are in a free space without boundaries or obstructions. In this case, the received signal power is given by:

$$P_R(d) = \frac{P_T \cdot G_T \cdot G_R \cdot \lambda^2}{(4\pi)^2 \cdot d^2 \cdot L} \tag{2.1}$$

This equation is the well-known *Friis free space equation.* Here, P_T stands for transmitted signal power, G for antenna gain (transmitter and receiver side), d for the distance between the antennas and L for the system loss. The ratio between transmitted signal power and received signal power is called the *Path Loss.* For isotropic antennas and no system loss this can be found to be:

$$PL = 20 \log \frac{4\pi}{\lambda} + 20 \log d \tag{2.2}$$

Which can be simplified to:

$$PL = 20 \log d_0 + 20 \log \frac{d}{d_0} \tag{2.3}$$

In reality however, there are more paths from the transmitter to the receiver than just a direct line of sight. Propagation is influenced by numerous kinds of objects. Three basic characteristics of propagation are:

- Reflection: from objects which are large compared to the wavelength.
- Diffraction: at sharp irregularities.
- Scattering: on objects in the medium which are small compared to the wavelength.

In complex environments an important distinction can be made when modelling path losses: the difference between large and small scale variations. For large scale variations we have $\mathrm{d}x \gg \lambda$ and $\mathrm{d}t \gg T_s$, where λ stands for wavelength and T_s for symbol time . Variations are considered small scale when $\mathrm{d}x \approx \lambda$ and $\mathrm{d}t \approx T_s$.

Large scale path loss

A lot of research has been done on modelling large scale path loss. Longley and Rice found a model which takes two-ray reflection and diffraction losses into account. This model has been adopted as America's Institute for Telecommunication Sciences (ITS) irregular terrain model and is valid from 40 MHz to 100 GHz.

Okumura made a model based on in-the-field measurements. With this model the average path loss can be calculated as follows:

$$L_{50}(\mathrm{dB}) = L_F + A_{mu}(f, d) - G(h_t) - G(h_r) - G_{AREA} \tag{2.4}$$

Where L_F is the free space path loss, A_{mu} the attenuation of the transmission medium relative to free space (can be found from Figure 2.2), $G(h_t)$

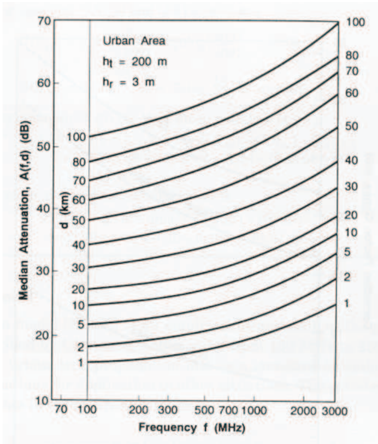

Figure 2.2: Relative medium attenuation according to Okumura

and $G(h_r)$ the transmitter and receiver height gain factor. G_{AREA} is an area-dependent correction factor. $G(h_t)$ and $G(h_r)$ can be found from the equations:

$$G(h_t) = 20 \log \frac{h_t}{200} \qquad 10m < h_t < 100m \tag{2.5}$$

$$G(h_r) = 10 \log \frac{h_r}{3} \qquad h_r < 3m \tag{2.6}$$

$$G(h_r) = 20 \log \frac{h_r}{3} \qquad 3m < h_r < 10m \tag{2.7}$$

Small scale fading and multipath effects

Where large scale fading models provide methods for predicting average signal strength at a distance d from a transmitter, small scale fading models give us insight on how the received signal will vary in short time intervals or with small distance variations.

Factors influencing small scale fading and multipath propagation can be characterized as follows:

- Rapid changes in signal strength (small distance or time interval).
- Random frequency modulation due to Doppler shifts.
- Time dispersion caused by multipath delays.

Four different kinds of small scale fading can be defined. When the coherence bandwidth (the approximate maximum bandwidth or frequency interval over which two frequencies of a signal are likely to experience comparable or correlated amplitude fading) of a channel is greater than the bandwidth of the signal, the channel fading is said to be 'flat'. Otherwise, the channel is said to be 'frequency selective'.

As a consequence of moving objects such as transmitters, receivers (a mobile phone in a car for example) or reflectors, doppler effects cause the signal to be spread in the frequency domain. The amount of spreading is modelled in the 'Doppler bandwidth'. From this bandwidth ($B_D = 2v/\lambda$) the coherence time can also be defined: $T_c = 1/B_D$. A channel is said to be 'fast fading' when the signal bandwidth is smaller than the doppler bandwidth. When the signal bandwidth is much larger than de doppler bandwidth, the channel is said to be 'slow fading'.

Since under normal conditions the path loss cannot be controlled, we can state that the designable parameters for system performance are transmitted power and minimum required SNR. Since transmitting power is limited in conformance with international radio regulations, SNR performance is the factor on which a new communication system must be judged.

2.4 Presentation of the system

When developing new communication systems, one should carefully consider the desired properties of the system. The goal of this project is the realization of a high capacity, robust, wireless communication system suitable for ad-hoc applications. As stated in subsection 2.3.1, bit error rate is a function of received SNR where SNR stands for the ratio between the desired signal power and the undesired (noise) signal power. It was also shown that received signal power is not only a function of antenna gain and distance between the antenna's but that fading also plays an important role.

Communication systems are dependent on conditions specific to their communication channel. For narrow-band systems, an in-band jamming signal or in-band fading is fatal for the system performance. To overcome this problem, ultra-wideband systems spread their signal over a very wide frequency range. Now, in-band jammers only influence a small part of their signal and correct retrieval of the signal is still possible.

2.4.1 Principles

The principle behind the spread spectrum technique used in FODMA can best be explained with a simple illustration. In Figure 2.3 a data sequence $m(t)$ is modulated with a broadband noise sequence $x(t)$ around frequency

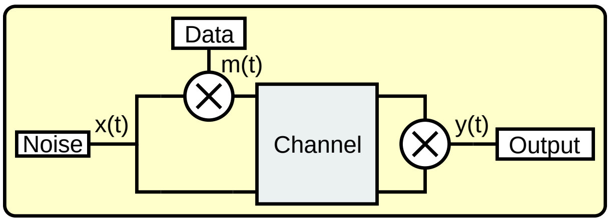

Figure 2.3: The principle behind spreading and despreading

ω. The bandwidth of $m(t)$ is just a fraction of the bandwidth of the noise sequence. The signal $m(t)x(t)$ is thus a broadband signal which contains the transmitted data sequence $m(t)$. When this modulated sequence and the unmodulated noise are transmitted over a channel to a receiver, the original data sequence can be obtained by the following operation:

$$\begin{aligned} y(t) &= (m(t) \cdot x(t)) \cdot x(t) \\ &= m(t) \cdot x^2(t) \end{aligned} \tag{2.8}$$

By rewriting $x(t)$ as it Fourier series representation, one can see that the signal consists of a series of cosine waves. Squaring $x(t)$ delivers a DC component and a component at twice the original center frequency.

$$\begin{aligned} y(t) &= m(t) \cdot cos^2(\omega t) \\ &= m(t) \cdot \frac{1}{2}(1 + cos(2\omega t) \end{aligned} \tag{2.9}$$

When $y(t)$ is low-pass filtered only the desired data sequence remains.

2.4.2 Methods

For despreading the original data sequence, the unmodulated noise sequence should be available at the receiver. One can use several methods to do this.

One method is transmitting the modulated noise and the unmodulated noise after each other. This method allows only half of the channel bandwidth to be used, in the other half no data are transmitted.

A second method is to delay the noise with a fixed delay τ_d and then add it to the modulated noise. At the receiver end the received signal is split, one branch is delayed with τ_d seconds. Both modulated and unmodulated noise are now available at the same time (τ_d seconds after receiving) for demodulation. This method uses the entire available bandwidth for transmitting data without interruption. Extensive research has been done on this principle for the optical domain (coherence multiplexing, [2], recently this method has

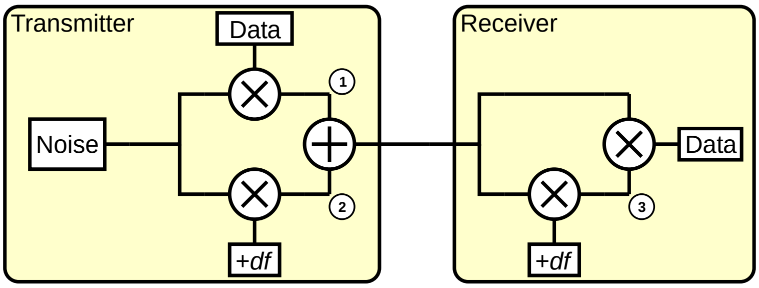

Figure 2.4: Schematic representation of the FODMA system

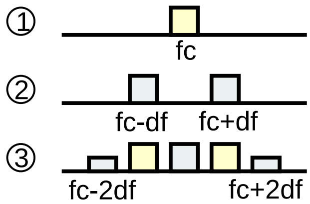

Figure 2.5: Frequency spectra of FODMA system

also been applied for a 2.4 GHz microwave communication system under the name of "Time Offset Division Multiple Access" (TODMA) [3] [4].

The third method, which is the subject of this masters thesis project uses the same principle as TODMA, but instead of a shift of the noise in the time domain, a shift in the frequency domain is applied. This system is called "Frequency Offset Division Multiple Access" (FODMA). An advantage of FODMA over TODMA is that the data required for demodulation are available instantaneously, no time offset has to be applied. Consequentially, FODMA is less susceptible to multipath effects than TODMA.

2.4.3 System description

Figure 2.4 is a schematic representation of the FODMA system. At the transmitter side one branch of the noise is modulated with the data in order to spread the data over the entire bandwidth of the noise. The other branch is shifted in frequency with $\mathrm{d}f$Hz, where $\mathrm{d}f > B_{data}$. The transmitted signal's spectrum is the sum of the modulated data and the frequency shifted versions of the noise. These frequency spectra are shown in Figure 2.5, one and two.

In the receiver, the incoming signal is split into two branches. One branch is shifted back in frequency to obtain the unmodulated noise at the original center frequency (Figure 2.5, spectrum three). By applying Formula 2.8 it can be seen that after lowpass filtering the output signal, the original data sequence will be available.

In practice, the relation between data bandwidth, offset frequency and spreading sequence bandwidth should fulfill the condition $B_{\text{data}} \ll df \ll B_{ss}$. The spectra in Figure 2.5 will overlap for the biggest part but this does not influence system principles.

Shang [5] found the output of the correlator to be:

$$\begin{aligned}
z(t) &= x^2(t)\cos^2(\omega_f t + \mu)\cos(\omega_0 t + \phi) \qquad (2.10)\\
&+ x^2(t)\cos^2(\omega_f t + \omega_0 t + \mu + \phi)\cos(\omega_0 t + \phi)\\
&+ 2m(t)\cdot x^2(t)\cos(\omega_f t + \mu)\cos(\omega_f t + \omega_0 t + \mu + \phi)\cos(\omega_0 t + \phi)\\
&+ \left[\int_{-\infty}^{\infty} n(t-\alpha)h(\alpha)\mathrm{d}\alpha\right]^2\cos(\omega_0 t + \phi)\\
&+ 2x(t)\cos(\omega_f t + \mu)\cos(\omega_0 t + \phi)\left[\int_{-\infty}^{\infty} n(t-\alpha)h(\alpha)\mathrm{d}\alpha\right]\\
&+ 2m(t)\cdot x(t)cos(\omega_f t + \omega_0 t + \mu + \phi)\cos(\omega_0 t + \phi)\left[\int_{-\infty}^{\infty} n(t-\alpha)h(\alpha)\mathrm{d}\alpha\right]
\end{aligned}$$

In this formula the most important parameters are: $x(t)$, the baseband representation of the spreading signal, which is in the case of FODMA a pseudo random noise source. $m(t)$ is the transmitted message, ω_f the carrier frequency of the system and ω_0, the applied frequency offset.

As a result of the squaring operations in the first two lines, an undesired delta pulse at frequency ω_0 is present at the output of the system. The desired output signal originates from the third line, which represents the demodulated message at the output, together with modulated versions around the center frequency and twice the center frequency.

The probability of error can be found from the SNR using Formula 2.11.

$$P_e = \frac{1}{2}\text{erfc}\left(\sqrt{\frac{SNR}{2}}\right) \qquad (2.11)$$

Shang found the performance for the single user case of FODMA to be:

$$P_{e,\min} = \frac{1}{2}\text{erfc}\left(\sqrt{\frac{1}{8+4\sqrt{7}}\cdot\frac{E_b}{N_0}}\right) \qquad (2.12)$$

For a fixed bandwidth system with limited output power, the energy per bit can be controlled by changing the ratio between information bandwidth B_d and transmission bandwidth B_{ss}. This ratio is called the processing gain and is given by Formula 2.13.

$$PG = 10\cdot\log\left(\frac{B_{ss}}{B_{data}}\right) \qquad [\text{dB}] \qquad (2.13)$$

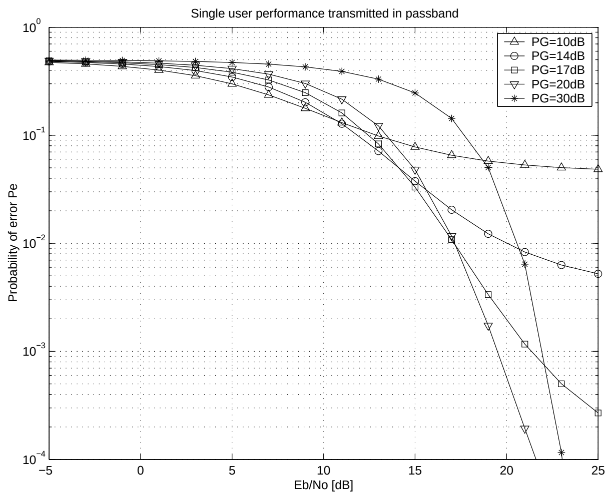

Figure 2.6: Single user performance of FODMA

The performance for various processing gains is plotted in Figure 2.6. It can be seen that for lower E_b/N_0, a lower processing gain is better.

FODMA is a *multiple access* technique. By assigning different frequency offsets to different users, the channel can be used by multiple users at the same time. Transmitted signals from other users will not significantly influence the own link since these signals will behave like uncorrelated noise for a receiver with a different frequency offset. However, since there are extra users the channel noise will increase and thus decrease system performance.

Chapter 3

Simulations

3.1 Introduction

The performance analysis of the FODMA system as presented by Shang in [5] shows the theoretical performance based on an idealized system model. In practice, however, microwave components are used to implement the required operations such as multiplication, phase shifting and adding. Since these components show non ideal behavior, it is useful to make simulations of the entire system in a microwave simulation program and examine the influence of these imperfections.

Simulations will be done at different levels of detail. First, the basics will be simulated using the simplest component models, later the complexity of the models will be increased.

The goal of the simulations is to verify the system's behavior with the theoretical performance as found by Shang. Noise will be added to the system in order to obtain the plots of bit error rate versus E_b/N_0.

3.2 Methods

The Agilent microwave simulation platform used throughout this study is Agilent's *Advanced Design System* (ADS). ADS is capable of Analog/RF simulation and convergence calculations, common circuit simulations, and Momentum field simulations. The RF simulation module can analyze the system using a variety of simulation engines including:

- DC analysis
- Transient analysis

- Harmonic balance

The FODMA system is analyzed using the Ptolemy transient analysis tool. This analysis solves the system of nonlinear ordinary differential equations, where the time derivatives are replaced with a finite difference approximation. For each time step the propagation of the input signals through the entire system is calculated and evaluated.

3.3 Models

The FODMA system has been simulated in ADS at different abstraction levels. The first model is a straightforward implementation of Figure 2.4 in ADS; no advanced component models are used. For multiplications, an ideal RF multiplier is chosen instead of a dedicated mixer model. For the RF multiplier the simulation time step is just as high as the spreading sequence's bandwidth ($T_{step} = 1/B_{ss}$). For more dedicated models the bandwidth increases drastically, therefore the simulation timestep must be much smaller, increasing the computing time for one simulation. The entire schematic is given in Figure 3.1. For the simulations as well as for the measurements, the assumption is made that the noise in the receiver and in the transmitter is negligible. Under this assumption, the ratio E_s/N_0 is fairly easy to determine:

$$\frac{E_s}{N_0} = \frac{P_{\text{tx}}}{P_{\text{noise}}} \tag{3.1}$$

To convert this to E_b/N_0 we can apply:

$$\frac{E_b}{N_0} = \frac{E_s \cdot T_{\text{symbol}}}{N_0 \cdot T_{\text{chip}}} \tag{3.2}$$

In ADS the "berMC4" functional block is used to determine the bit error rate as a function of E_b/N_0. This block determines the signal power at the output of the transmitter and the power of the added noise. The BER is determined by comparing the original transmitted data with the received data. For a high reliability of the obtained BER values, the number of errors counted should be considerable. As a consequence of this, simulations of the system with high values for E_s/N_0 will are time consuming, since the number of bits to be transmitted is quite high. For example, at a BER of $1 \cdot 10^{-4}$ the number of transmitted bits should be around $1 \cdot 10^6$.

3.3.1 First model

The components used in this model are described below:

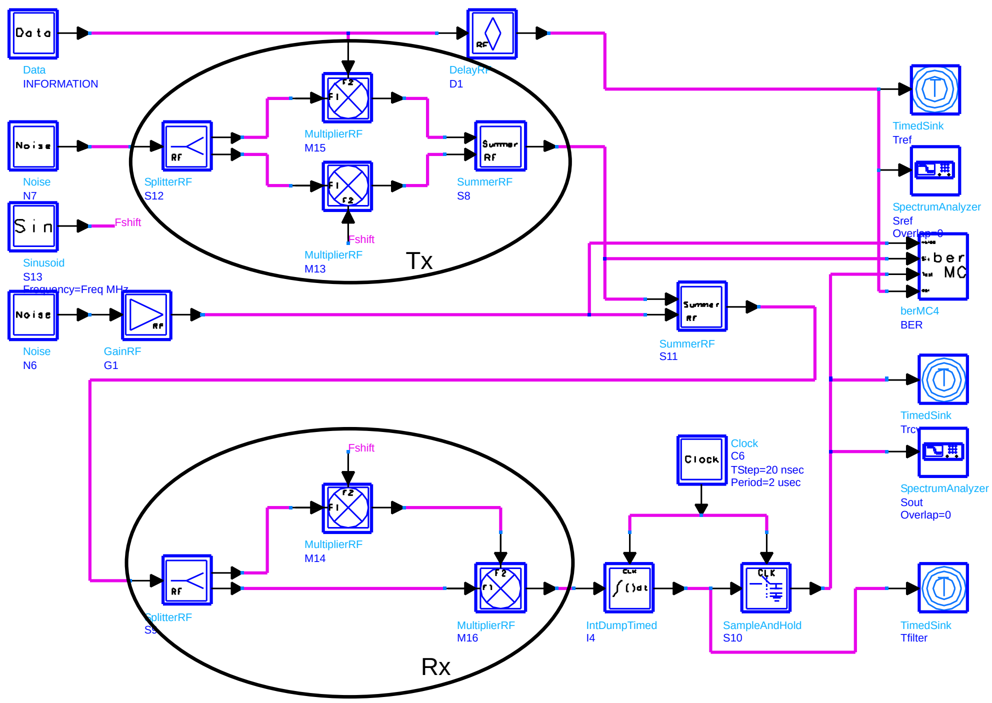

Figure 3.1: First ADS model of FODMA testbed

Noise

The two noise sources both generate 50 MHz wide gaussian noise. The probability density function of this noise is:

$$f(v) = \frac{1}{\sqrt{2\pi V_B^2}} \cdot e^{-\frac{(v-V_A)^2}{2V_B^2}} \tag{3.3}$$

During the simulations, V_A is set to zero and V_B is set to one. The noise generated is a pseudo random noise sequence, which is dependent on the initial state of the noise seed. This seed can be a fixed value for all simulations, but in this case, for each simulation a random value for the seed is chosen.

Data

The data block generates a pseudo random, NRZ data sequence. The bit-time can have values that are an integer multiple of the simulation step-time. The initial state of the random data generator can be user-defined using the *default seed*. When the default seed is chosen to be zero, each simulation will have a random start seed.

MultiplierRF

The MultiplierRF block is a straightforward model of an RF multiplier. The block can be used as an up-converter, down-converter or double-sideband modulator. When one of the inputs is a baseband signal, which is the case in the FODMA simulation, the block can only be used as a double-sideband modulator.

The output of the MultiplierRF block, when working in double-sideband mode is given by:

$$f_{c3} = \max(f_{c1}, f_{c2}) \tag{3.4}$$

$$v_3(t) = \frac{1}{2}v_1(t)v_2(t) + \frac{1}{2}v_1(t)v_2^*(t) \tag{3.5}$$

$$\begin{aligned} v_k(t) &= \mathrm{Re}\left\{v_k(t) \cdot e^{\mathrm{j}2\pi f_{ck} t}\right\} \\ &= v_{Ik}(t) + \mathrm{j}v_{Qk}(t) \end{aligned} \tag{3.6}$$

where $V_k(t)$ are the complex envelopes of the signals at the input pins 1 and 2 and output pin 3. In practice, RF mixers are used for multiplying operations. Real mixers are nonlinear components, which introduce higher order frequency components into the signal.

3.3.2 Second model

In the second model, the influence of using a dedicated mixer model has been investigated. The MultiplierRF component described above does not introduce higher order components, while in practice, higher order components are introduced. These higher order frequency components originate from non-idealities in a mixer, such as signal leakage from one port to another. To take these effects into account, the MultiplierRF component has been replaced with a MixerRF component, which is described below.

MixerRF

The MixerRF block is an advanced version of the MultiplierRF block. The main difference is that leakage factors (RF to IF rejection, image rejection and LO rejection) can be given. Again, $V_k(t)$ are the complex envelopes of the signals at port 1, 2 and 3. Now, the output is given by:

$$v_3(t) = g_{mix}v_{sig}v_{lo} + v_{leakRF} + v_{leakLO} + v_{leakImage} \tag{3.7}$$

The rejection factors are set in accordance with manufacturers specifications for the mixers to be used in the testbed.

USampleRF

The detailed simulations have one big disadvantage. The simulation time step must be smaller that $4 \cdot 10^{-11}$ seconds instead of the $2 \cdot 10^{-8}$ which was needed for the first model. Every simulation will thus take 500 times longer. These simulations can therefore only be used for low bit error rates.

Since the spreading sequence generated in the noise block only has a timestep of $2 \cdot 10^{-8}$, this signal has to be upsampled. For this operation the USampleRF component has been used.

3.3.3 Third model

In our testbed, the noise that has to be generated for spreading the data signal is not gaussian noise. In fact, it is a polar, pseudo-random data sequence around the desired 2.4 GHz. The third simulation model differs from the first only in the generation of the spreading sequence. The noise which is generated in the noise block is amplified and limited to a fixed amplitude, this way the signal has the same properties as the signal which will be used in the measurements.

3.4 Results

First, a proof-of-concept simulation has been performed, using the model as given in Figure 3.1. The system has been simulated with a processing gain of 17dB without channel noise. In Figure 3.2 the output of the system is given at three points in the receiver. The first point is the output of the last mixer, the second is after the integrator and the third after the sampler.

As can be seen, the output of the system shows the expected behavior: when the frequency offset in the receiver is the same as in the transmitter, the original data are recovered, with a different frequency (in this case a 5 MHz offset in the transmitter and a 6 MHz offset in the receiver), only noise is received, resulting in a 50 percent bit error rate.

3.4.1 Frequency spectra

For comprehending the entire system's behavior, it is useful to have a good insight not only in the time domain behavior of the system but also in the frequency domain behavior. For this purpose, the frequency spectra at some relevant points in the system have been determined by simulation. These spectra are determined with the second simulation model, since this model gives the most detailed results.

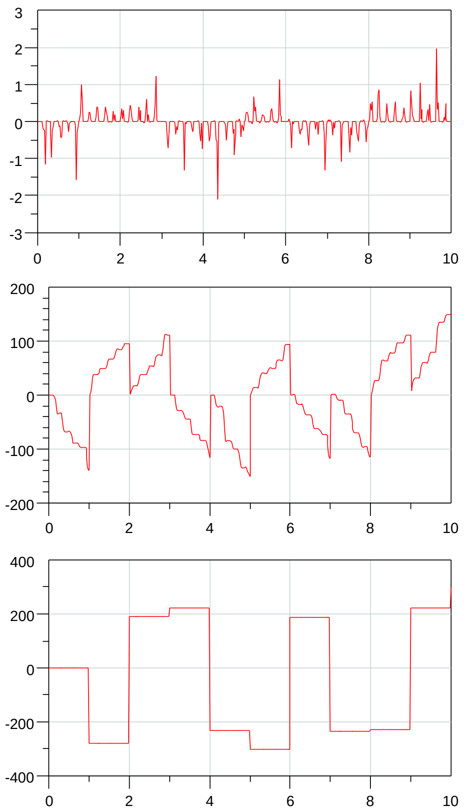

(a) Correct frequency offset

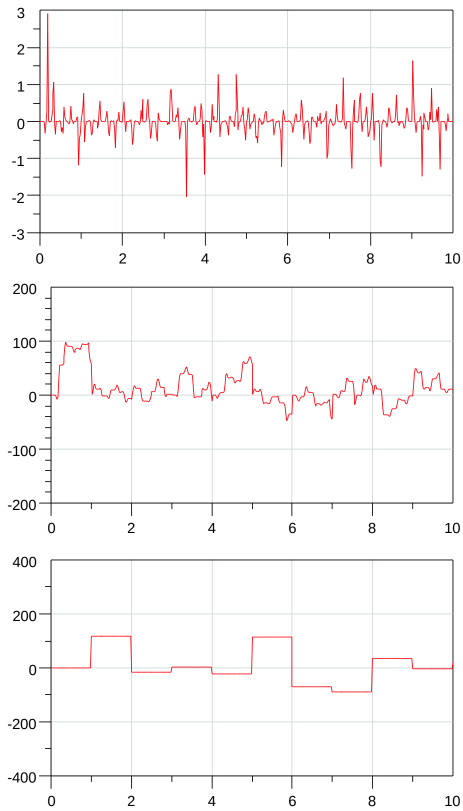

(b) Frequency offset mismatch

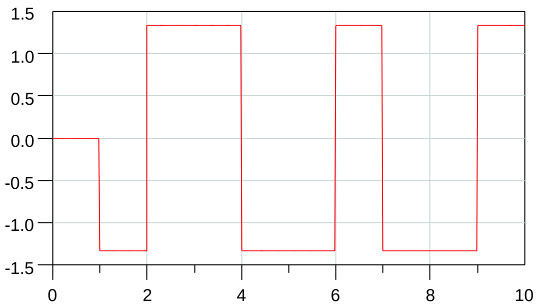

(c) Input data

Figure 3.2: FODMA output

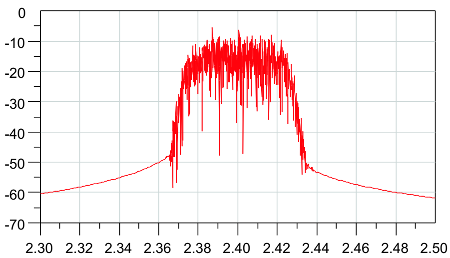

(a) Spreading sequence

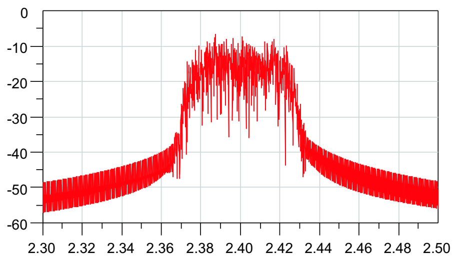

(b) Spreading sequence × data

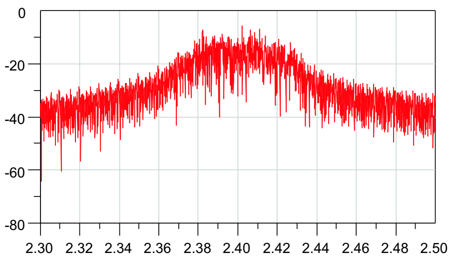

(c) Spreading sequence × offset frequency

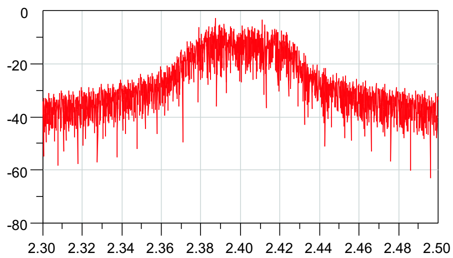

(d) Transmitter output

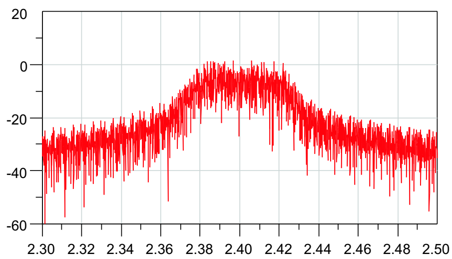

(e) Received signal × offset frequency

Figure 3.3: Simulated spectra in the system

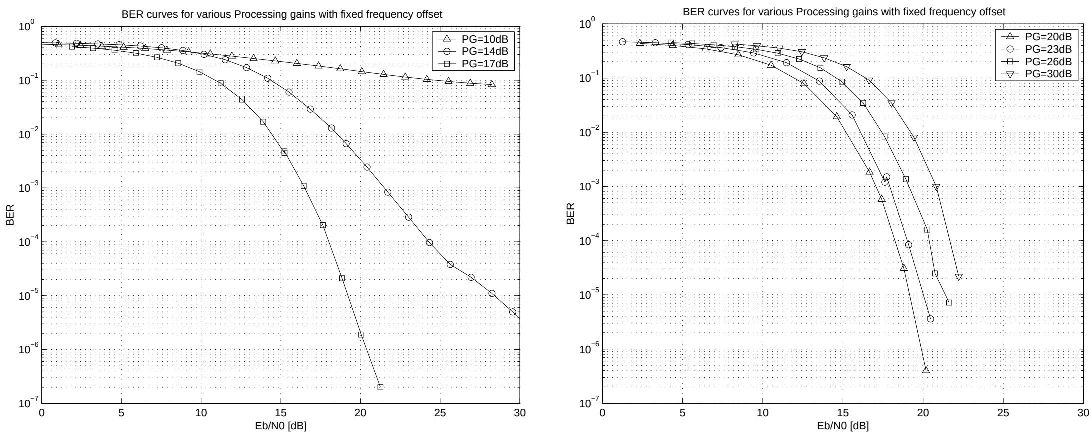

(a) (b)

Figure 3.4: BER curves for various processing gains, model 1

Later, when the system has been realized, these spectra will also be measured.

3.4.2 BER curves

The main issue of the system simulation is determination of the BER curves for various processing gains. In Shang's theoretical performance analysis, for each value for the processing gain, an error floor was found. Also, for each value of E_b/N_0 an optimal value for the processing gain was determined.

First model

In Figure 3.4 the simulation results of the first model are presented. It can be seen that for low processing gains an error floor occurs. The error floors for the higher processing gains are present, but could not be calculated as a consequence of the extremely long simulation times.

When comparing these simulation results with the theoretical results as found by Shang (Figure 2.6) , it can be seen that the basic behavior is equal, but there is not an exact fit. The high-processing gain simulations match reasonably well. For low processing gain values the theoretical performance is better than the simulated. For higher values it is the other way around.

A possible explanation for this difference is the statistical properties of the noise. In this simulation, a noise with gaussian amplitude distribution is used. In the theoretical performance analysis, there is also a random phase of the noise, which is not the case in the simulations.

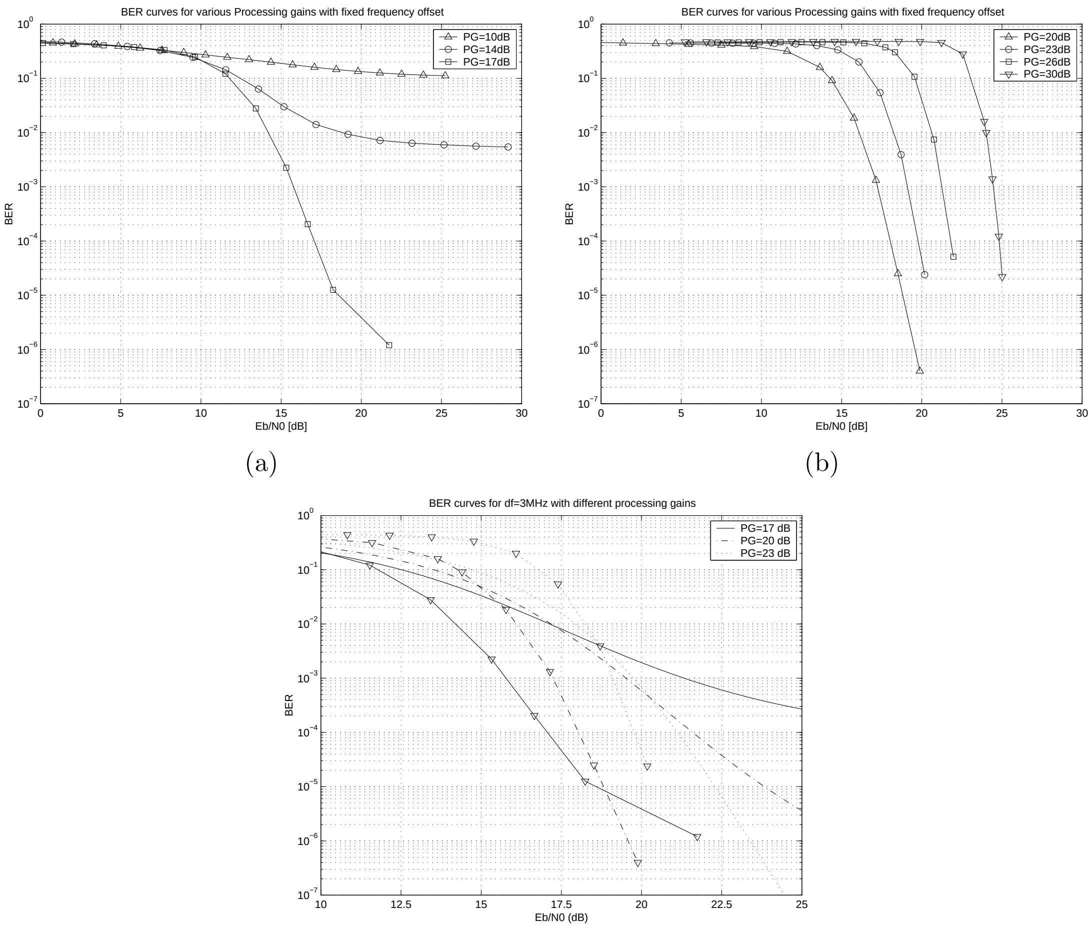

Figure 3.5: BER curves for various processing gains, model 3

Second model

The second model has only been used for generating the frequency spectra as shown in Figure 3.3. An offset frequency of 3 MHz has been applied. BER simulations could not be done because of the long simulation times involved.

Third model

The spreading sequence of the third model is a clipped version of the noise generated by the noise block, in order to have the same characteristics as the noise which will be used in the testbed. In Figure 3.5 the results of this simulations are shown.

In Figure 3.5(c) the analytical results are shown together with the results found by simulation model 3. The curves with the triangle marks are obtained by simulation, the unmarked curves are analytical results. Surprisingly these results match reasonably well with the analytical results. This is remarkable since in the theoretical model a gaussian noise source is used as a spreading sequence.

Chapter 4

RF system design

The main goal of this master thesis project is the realization of a FODMA testbed. In the preceding chapters the FODMA system has only been described from a theoretical point of view. In practice however, components are used which do not show ideal behavior. For example, a coax cable of one meter introduces a phase shift of around 12λ and an attenuation of almost 1.5 dB for signals around 2.4 GHz.

In this chapter some basic RF design fundamentals are explained. Furthermore the characteristics and operation of RF mixers is explained.

4.1 Noise analysis

Noise is the enemy of most electrical engineers. It degrades system performance and, therefore, is a big issue. FODMA uses this 'enemy' as a bearer of the signal. Like in any other system, also unwanted noise is present. Thermal agitation of electrons is a main source of noise. The noise power as a consequence of this phenomenon is given by:

$$P_{TN} = kTB_N \tag{4.1}$$

where k is Bolzmann's constant, T is temperature in kelvin and B_N is the system's bandwidth. The noise contribution of a component is typically given by its noise factor:

$$F = \frac{S_{ni}}{S_{no}} \tag{4.2}$$

or the noise figure:

$$NF = 10 \log \frac{S_{ni}}{S_{no}} \qquad [dB] \tag{4.3}$$

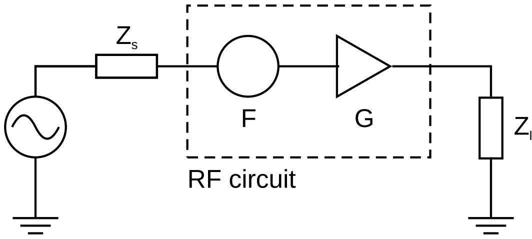

Figure 4.1: Equivalent circuit for an RF component

where S_{ni} stands for available SNR at the input and S_{no} for available SNR at the device output.

In Haykin [6], the Noise Figure is defined as: "*the ratio of the total available output noise power (due to the device and the source) per unit bandwidth to the portion thereof due solely to the source*".

For low-noise devices, the values of the noise factor are close to unity, which makes comparison with other low-noise devices difficult. For these cases the noise characteristics can be described in an alternative way, using the *equivalent noise temperature*. First, the RF circuit is decomposed into two elements: an ideal amplifier with gain G and a noise source (F) as shown in Figure 4.1.

When the in- and output impedances are matched to the source- and load impedance, the available noise power at the input of this equivalent circuit is:

$$N_s = kTB_N \tag{4.4}$$

The noise power contributed by the device itself can be given by:

$$N_d = GkT_eB_N \tag{4.5}$$

The variable which is introduced here, T_e, is called the equivalent noise temperature. With this new definition of N_d, the output noise power can be given by:

$$\begin{aligned} N_0 &= GN_s + N_d \\ &= Gk(T + T_e)B_N \end{aligned} \tag{4.6}$$

from which we can derive

$$\begin{aligned} F &= \frac{N_0}{GN_s} \\ &= \frac{T + T_e}{T} \\ T_e &= T(F-1) \end{aligned} \tag{4.7}$$

When cascading components, the noise factor of the entire system can be determined as follows:

$$\begin{aligned} N_o &= G_1 G_2 N_s + G_2 N_{d1} + N_{d2} \\ &= G_1 G_2 k \left(T + T_1 + \frac{T_2}{G_1} \right) B_N \end{aligned} \tag{4.8}$$

When comparing equation 4.8 with equation 4.6 we can see that the equivalent noise temperature of the cascaded system is given by:

$$T_e = T_1 + \frac{T_2}{G_1} \tag{4.9}$$

This can be expanded for an arbitrary number of networks to:

$$T_e = T_1 + \frac{T_2}{G_1} + \frac{T_3}{G_1 G_2} + \ldots + \frac{T_n}{\prod_{i=1}^{n-1} G_i} \tag{4.10}$$

or, rewritten to the noise figure F as:

$$F_N = F_1 + \frac{F_2 - 1}{G_1} + \frac{F_3 - 1}{G_1 G_2} + \ldots + \frac{F_n - 1}{\prod_{i=1}^{n-1} G_i} \tag{4.11}$$

This equation is known as the *Friis equation for cascaded noisy systems.* From this equation it can be seen that the first components in a chain with positive gains have the biggest influence on the overall noise performance. It is for this reason that the front-end amplifier in a receiver should be a low-noise component.

4.2 Frequency shifting operations

A common operation in communication electronics is the shift of a signal from one frequency to another. This frequency shift can be implemented by multiplying the desired signal with the desired shifting frequency:

$$\begin{aligned} s(t) &= m(t) \cos(2\pi f_c t) \cdot \cos(2\pi f_s t) \\ &= \frac{m(t)}{2} \left[\cos(2\pi (f_c - f_s) t) + \cos(2\pi (f_c + f_s) t) \right] \end{aligned}$$

RF signals can be multiplied using an RF mixer. A mixer uses a nonlinear device to perform the actual multiplication. Most common are diode and transistor mixers.

The DC V-I characteristic of a diode can be expressed as:

$$I(V) = I_s(e^{\alpha V} - 1) \tag{4.12}$$
$$\alpha = \frac{q}{nkT} \tag{4.13}$$

Let the diode voltage be:

$$V = V_0 + v \tag{4.14}$$

where V_0 is a DC bias voltage and v is a small AC signal voltage. When expanding 4.12 in a Taylor series about V_0 we get:

$$I(V) = I_0 + v \left.\frac{\mathrm{d}I}{\mathrm{d}V}\right|_{V_0} + \frac{1}{2}v^2 \left.\frac{\mathrm{d}^2 I}{\mathrm{d}V^2}\right|_{V_0} + \ldots \tag{4.15}$$

The constant I_0 is a consequence of the applied DC bias. The first and second derivative are found to be:

$$\left.\frac{\mathrm{d}I}{\mathrm{d}V}\right|_{V_0} = \alpha I_s e^{\alpha V_0} = \alpha(I_0 + I_s) = G_d = \frac{1}{R_j} \tag{4.16}$$
$$\left.\frac{\mathrm{d}^2 I}{\mathrm{d}V^2}\right|_{V_0} = \left.\frac{\mathrm{d}G_d}{\mathrm{d}V}\right|_{V_0} = \alpha^2(I_0 + I_s) = \alpha G_d = G'_d \tag{4.17}$$

now, equation 4.15 can be rewritten as:

$$I(V) = I_0 + i = I_0 + vG_d + \frac{v^2}{2}G'_d + \ldots \tag{4.18}$$

which is known as the *small-signal approximation* for diode behavior.

In mixers, the v^2 term is used to produce sum and difference frequencies of a low-level RF signal and an RF local oscillator (LO) signal.

$$f_{IF} = f_{RF} \pm f_{LO} \tag{4.19}$$

The simplest type of mixer is the *single-ended mixer*. RF and LO signals are typically given by:

$$v_{RF}(t) = v_r \cos\omega_r t \tag{4.20}$$
$$v_{LO}(t) = v_0 \cos\omega_0 t \tag{4.21}$$

When these two signals are combined and fed into a diode, the v^2 term will perform the desired frequency mixing operation:

$$\begin{aligned} i &= \frac{G'_d}{2}\left(v_r \cos\omega_r t + v_0 \cos\omega_0 t\right)^2 \\ &= \frac{G'_d}{2}\left(v_r^2 \cos^2\omega_r t + 2v_r v_0 \cos\omega_r t \cos\omega_0 t + v_0^2 \cos^2\omega_0 t\right) \\ &= \frac{G'_d}{4}[v_r^2 + v_0^2 + v_r^2 \cos 2\omega_r t + v_0^2 \cos 2\omega_0 t \\ &\quad +2v_r v_0 \cos\left(\omega_r - \omega_0\right)t + 2v_r v_0 \cos\left(\omega_r + \omega_0\right)t] \end{aligned} \tag{4.22}$$

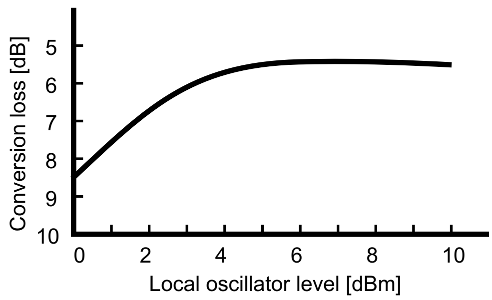

Figure 4.2: Typical conversion loss vs LO drive for 7dBm mixer

The terms of interest are those of frequency $\omega_r \pm \omega_0$, DC, $2\omega_0$ and $2\omega_r$ terms can be filtered out. Also the terms in the output that are generated by the v term can be filtered out. From the equations above, it can easily be seen that not all input power is converted to the desired output signals. The ratio between these powers is called the *conversion loss*, and is given by:

$$L_c = 10 \log \frac{\text{available RF input power}}{\text{IF output power}} \text{ dB} \tag{4.23}$$

The conversion loss is dependent on the LO input power. The function of this LO drive is to switch the diode(s) in the mixer fully on and off, for the lowest possible distortion. The required LO drive power is a design parameter, mixers are available in a wide range of required LO powers. Most common are level 7 mixers, which require 7 dBm LO input power.

When a mixer is driven at its required power, conversion loss is minimal. Small changes in driving power, around the designed power level, are not critical. A typical conversion loss vs. LO drive plot is given in Figure 4.2.

4.3 Distortion

When the Taylor expansion of diode behavior (Eq: 4.15) is generalized, we can write the transfer characteristics of any device as:

$$y(t) = \alpha_1 x(t) + \alpha_2 x^2(t) + \alpha_3 x^3(t) + \cdots \tag{4.24}$$

When the input consists of a single sinusoidal wave $x(t) = A\cos(2\pi f t)$, the output of this system will be (ignoring fourth and higher order terms):

$$\begin{aligned} y(t) &= \frac{1}{2}\alpha_2 A^2 + (\alpha_1 A + \frac{3}{4}\alpha_3 A^3)\cos(2\pi f t) \\ &\quad + \frac{1}{2}\alpha_2 A^2 \cos(4\pi f t) + \frac{1}{4}\alpha_3 A^3 \cos(6\pi f t) \end{aligned} \tag{4.25}$$

This equation can be decomposed into fundamental, second harmonic and third harmonic frequency terms. Their amplitudes are:

Fundamental: $\alpha_1 A + \frac{3}{4}\alpha_3 A^3$

Second harmonic: $\frac{1}{2}\alpha_2 A^2$

Third harmonic: $\frac{1}{4}\alpha_3 A^3$

With these amplitudes the second- and third-order harmonic distortion is found to be:

$$D_2 = \frac{\frac{1}{2}\alpha_2 A}{\alpha_1 + \frac{3}{4}\alpha_3 A^2} \tag{4.26}$$

$$D_3 = \frac{\frac{1}{4}\alpha_3 A^2}{\alpha_1 + \frac{3}{4}\alpha_3 A^2} \tag{4.27}$$

When the input is changed from one single sine wave to two waves with different frequencies, the third-order term $\alpha_3 x^3(t)$ gives rise to intermodulation products at the frequencies $2f_1 \pm f_2$ and $2f_2 \pm f_1$. These frequency components have the following amplitudes:

$2f_1 \pm f_2$: $\frac{3}{4}\alpha_3 A_1^2 A_2$

$2f_2 \pm f_1$: $\frac{3}{4}\alpha_3 A_1 A_2^2$

From the foregoing section we may conclude that distortion is inevitable when using diode mixers. However, by using multiple diodes in a star- or ring configuration spurious products can be suppressed. For the FODMA testbed, double balanced diode mixers are used.

4.4 Power splitter

A power splitter is a three-port network with the task to split the power at the input and divide it over the two outputs. If all ports are matched, the scattering matrix of a three-port network is given by:

$$[S] = \begin{bmatrix} 0 & S_{12} & S_{13} \\ S_{12} & 0 & S_{23} \\ S_{13} & S_{23} & 0 \end{bmatrix} \tag{4.28}$$

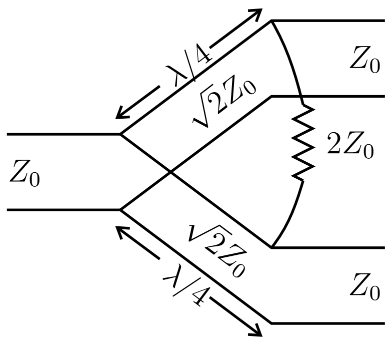

Figure 4.3: Transmission line circuit of a Wilkinson power divider

$$|S_{12}|^2 + |S_{13}|^2 = 1 \tag{4.29a}$$
$$|S_{12}|^2 + |S_{23}|^2 = 1 \tag{4.29b}$$
$$|S_{13}|^2 + |S_{23}|^2 = 1 \tag{4.29c}$$
$$S_{13}^* S_{23} = 0 \tag{4.29d}$$
$$S_{23}^* S_{12} = 0 \tag{4.29e}$$
$$S_{12}^* S_{13} = 0 \tag{4.29f}$$

From equations 4.29d…4.29f it follows that at least two of the three parameters (S_{12}, S_{13}, S_{23}) must be zero, which is in contradiction with 4.29a…4.29c. It follows that a three-port network cannot be lossless, reciprocal and matched at all ports at the same time.

Wilkinson developed a three-port power divider (Figure 4.3) which is lossless in power dividing, while being matched at all ports. It's S-matrix is given by:

$$[S] = -\frac{j}{\sqrt{2}} \begin{bmatrix} 0 & 1 & 1 \\ 1 & 0 & 0 \\ 1 & 0 & 0 \end{bmatrix} \tag{4.30}$$

It can be seen from this matrix that this divider has ideal isolation from port two to port three and vice-versa. The power offered at port one is equally divided over the two output ports, without losses. However, this device is not lossless; when power is applied to port two or three, only half of the power appears at port one. The other half of the power is dissipated in the internal resistance between port two and three.

Since a single Wilkinson divider has a small operating bandwidth as a consequence of the $1/4\lambda$ lines involved, for a broader operating range several Wilkinson dividers have to be cascaded.

Chapter 5

Realization

5.1 Setup

Combining the knowledge from the simulations and the RF circuit design theory, components have been collected to realize the testbed. These components had to be compatible with the instruments already available in the lab and had to comply with high standards. First, a schematic drawing has been made of the entire system. In the drawing, rough values of the power levels in the entire system are given. These values have been derived from the required input powerlevels of each component. This drawing is given in Figure 5.1. In the following subsections the motivation for the use of each component is given.

5.1.1 Vector signal generator

The input signals to the system are generated by various signal generators. The signal used as a spreading sequence in the transmitter is generated by an Agilent vector signal generator which is capable of generating up to 50 MHz wide pseudo-random data sequence at any center frequency up to 6 GHz. A wide range of signal formats is available. In the FODMA system a BPSK constellation diagram is chosen. The center frequency is 2.4 GHz. The data is generated by a PN23 pseudo random noise generator.

5.1.2 Mixers

The entire transmitter and receiver chain of the FODMA system contains four frequency mixers, which have to perform three unique tasks. In the transmitter, the data which are to be transmitted have to be modulated on

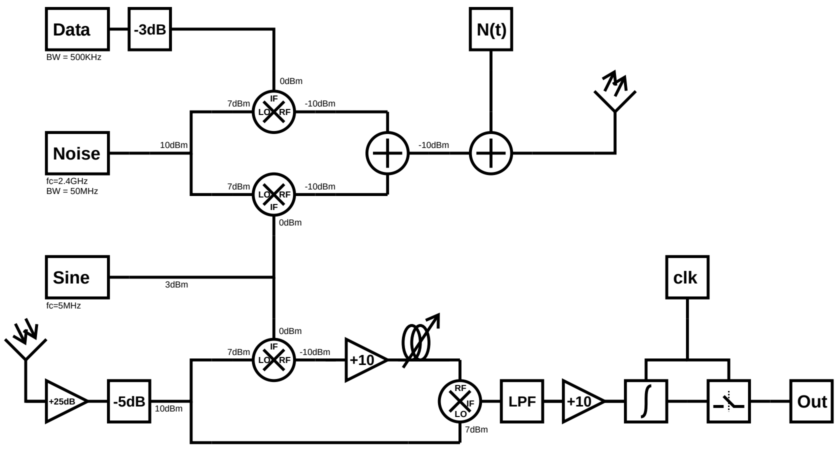

Figure 5.1: Schematic drawing of the FODMA system

the broadband noise carrier. Also, the reference noise has to be shifted in frequency.

At the receiver side, one mixer performs the same frequency shifting operation as in the transmitter. The task of the fourth mixer is to despread the transmitted data back to the baseband. For the best performance, a linear operation in the desired frequency range is desired. Also low distortion and low third-order intermodulation products are required.

The operating frequency of the mixers in the RF band is around 2.4 GHz. For the characteristics around this center frequency to be maximally flat, mixers with a much wider bandwidth are chosen. The IF port should work from DC to at least the largest required offset frequency ($df \gg B_{\text{data}}$). Finally, a mixer from Minicircuits has been chosen (ZX05-30W, [7]), which has an LO/RF frequency range from 300 to 4000 MHz and an IF range from DC to 950 MHz. The required LO drive power is +7 dBm.

5.1.3 Splitters

The main issue in splitters is, as in other components, low losses. From theory we know that Wilkinson power dividers show ideal splitting behavior. The only disadvantage of a single Wilkinson structure is the small bandwidth. Minicircuits has developed a ultra wide band power splitter (ZN2PD2-50, [8]), which consists of a series of seven Wilkinson dividers. The bandwidth of this splitter ranges from 500 to 5000 MHz. Due to losses in the materials and connectors, the insertion loss of this splitter is not only the -3dB because of the split, but there is an additional loss of 0.8-1.4dB.

A logical question at this point can be: Why not choose a power splitter which is designed for a small band around 2.4 GHz? The easy answer is that there were already two splitters of this type available. The more satisfying answer is that it is more profitable for the microwave communication lab to invest in a device which is suitable for a wider frequency range, so that it can be used for other applications as well.

5.1.4 Amplifiers

From the Friis equation for cascaded systems (4.11) it follows that the first component in a cascaded system with positive gains dominates the overall noise performance of a system. For this reason it is important to pick a very low-noise high gain amplifier as front-end amplifier. It can be deduced from Figure 5.1 that the power level at the output of the amplifier should be around +10 dBm. The input power level will be somewhere around -10 dBm, so at least 20 dB amplification is needed.

With the noise figure and bandwidth requirements, eventually the Minicircuits ZRL-2400LN [9] amplifier has been selected. This amplifier has a 25 dB gain, with a noise figure of 1.2 dB typical. The frequency range of this amplifier ranges from 1000 to 2400 MHz, which is sufficient for our system.

From Figure 5.1 it can also be seen that in the receiver, a second amplifier is needed. This amplifier compensates for the conversion loss in the frequency-shifting mixer. Operation is possible without this amplifier but then the total output power would be lower than -20 dBm while when using this amplifier, the output level will be higher.

The desired RF input level of the last mixer in the system is 0 dBm, thus a 10 dB amplifier is needed. From the IC Design (ICD) group, a Minicircuits 10 dB amplifier of the type ZJL-7G [10] could be borrowed. This amplifier has a frequency range from 20 to 7000 MHz with a noise figure of 5 dB.

After filtering of the output, another +10 dB amplification is applied, which gives us an output signal between 10 and 100 mV. Since the signal of interest is a baseband signal, this amplifier needs to amplify from DC to at least the signal's bandwidth. The ICD group also supplied an EG&G parc wide-band preamplifier from DC to 70 MHz, with a selectable gain of 10 or 20 dB.

5.1.5 Filters

From equation 2.10 it follows that the output of the correlator contains not only the desired baseband signal but also higher frequency components. These components are filtered out with two separate filters. The first filter is located directly after the correlator. This filter is a Minicircuits lowpass filter (SLP-2.5, [11]) which filters out frequencies above 2.5 MHz. From 3.8 to 5 MHz, the losses are more than 20 dB, above 5 MHz more than 40 dB.

The second filter is an active Krohn-Hite filter (model 3202). It has a variable cutoff frequency between 20 Hz and 2 MHz with slopes of 24 dB/octave. Despite of noise considerations, this filter is placed before the last amplifier. This is to prevent overloading the final amplifier.

5.1.6 Other components

For optimal demodulation, it is important that the information bearing noise arrives in phase with the reference noise at the correlator. This can be obtained by inserting a coaxial phase shifter in one of the branches of the receiver.

When determining BER curves as a function of signal power over noise power, it must be possible to control the signal- or the noise power. The added noise should not be correlated to the transmitted signal. Since there are not two signal generators capable of generating a 50 MHz noise signal available in the microwave lab, another solution for generating the 'channel noise' had to be found. The method applied in my measurements uses the fact that the correlation time of a (pseudo-)random noise source is very short. The noise generated by the vector signal generator is split. One branch is used as a spreading sequence in the transmitter, the other branch is delayed by sending it over 40 meters of coax cable to obtain a delay of approximately 200 ns. This delay equals ten bit-times of the noise source, which is enough for the noise to be uncorrelated with its time-shifted version. To compensate for the signal attenuation in the cables, two amplifiers of the type MAX2242/3 are used. These amplifiers provide a 28.5 dB gain and compensate for the 1.5 dB/m cable loss. The power level of the noise can be controlled by two cascaded variable attenuators, the HP 8494B/11dB and the HP 8495B/70dB. With these attenuators, the channel noise power can be attenuated in steps of 1 dB from 0 to 81 dB.

All cabling is standard RG316 50-ohms cable with SMA connectors.

5.1.7 Equipment

Besides the components described in the sections above, the following equipment has been used:

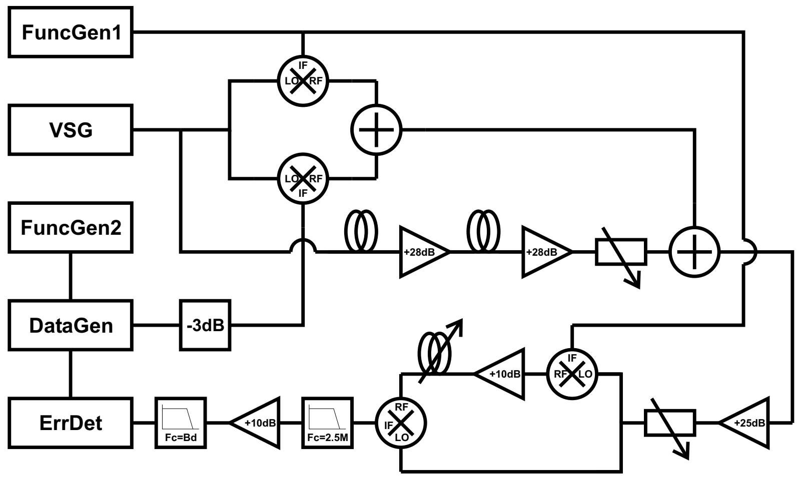

Figure 5.2: Schematic drawing of the FODMA testbed

Function	**Component**
Vector signal generator	Agilent E4438C ESG
Data generator	HP 3762A
Error detector	HP 3463A
Function generator 1	Rhode&Schwartz SMS
Function generator 2	HP 33120 Function Generator
Spectrum analyzer	HP 8593E
Oscilloscope	HP 54600A
Phase shifter	Nardia 3752

With these components the setup as given in Figure 5.2 has been built.

5.2 Measurements

Before presenting the first measurement results a short introduction of the performed measurements and measurement techniques is given.

For determining BER curves as a function of the available signal to noise ratio, some important definitions have to be stated first.

Output signal power: The power measured directly at the output of the transmitter in a 50 MHz band around 2.4 GHz.

Channel noise power: The power of the noise added to the output signal in a 50 MHz band around 2.4 GHz.

C/N: The ratio between the Output signal power and the channel noise power.

SNR: C/N plus the processing gain.

5.2.1 Power levels

For power measurements, a spectrum analyzer has been used. In order to make an accurate measurement, the signal of interest is averaged over 100 samples before showing on the display. Since the dynamic range of the signals is very large, the spectrum analyzer is set to a log (dB) display mode. However, we must be careful with the measurement results obtained this way for the following reason: the log of the average is not equal to the average of the log! Due to the log scaling, noisy peaks are compressed while dips are expanded towards minus infinity dB! This causes the measured average power in a frequency band to be lower than the actual value. For noisy signals, a fixed correction factor of +2.51dB has to be applied [12].

At frequencies around 2.4 GHz, cable losses are of major influence. Cable loss per meter, is 1.5dB.

The correction factor and losses mentioned above are only of interest when we are interested in absolute power levels at in- or output ports of the components used. For the SNR measurements they are of no interest, as long as the measurements are performed with the same set of cables.

5.2.2 BER measurements

For making BER measurements, we need a device which is capable of generating a NRZ (pseudo-)random data sequence that can serve as data input for the transmitter, and a receiver which is capable of comparing the output data of the receiver with an internally generated and synchronized version of the same sequence. For this goal, the HP 3762A data generator and HP 3463A error detector are used. These devices are capable of handling datarates between 1 Kbps and 150 Mbps. For statistically reliable results, the BER is calculated after counting a fixed number of errors which is in our case 100 errors.

5.3 Results

After assembling the entire system, the measurements could begin. First, the measured frequency spectra are presented, then the BER measurements are dealt with.

5.3.1 Frequency spectra

Power spectra at all important points in the system are measured to check whether they match with our predictions. In Figure 5.3 the spectrum at the transmitter side is shown. As can be seen in Figure 5.3(b), the spreading sequence is not exactly 50MHz wide but a little broader, with small sidelobes. Raised cosine filtering with a factor $alpha = 0.1$ is applied to reduce the amount of power in the sidelobes. Furthermore it is important to note that the 2.4GHz carrier is present in the spreading sequence. In Figure 5.3(d) the shifted versions of the carrier frequency can be seen at $f_c \pm 3MHz$. These carrier frequencies are of major importance to the performance of the system, as will be shown next.

In Figure 5.4 the spectrum at the receiver's side is shown. In Figure 5.4(a) the frequency offset is applied again. It is clear that the carrier frequency is present again at 2.4GHz. Not so easily seen are the peaks at 2400 ± 3 and ± 6 MHz. These peaks mix back in the last mixer to the integer multiple frequencies of 3 MHz in Figure 5.4(b). Not shown in this figure are the higher frequency components that are predicted by Equation 2.10, however, they are present around 2.4 and 4.8 GHz. The first filter removes these high frequencies. After this first filter, the second filter, which is matched to the data bandwidth removes the other higher frequency components. As can be seen in Figure 5.4(f) the 3MHz component is effectively suppressed by this filtering, which makes detection of the original signal possible using the error detector.

The measured spectra match our predictions, based on the simulation results (Figure 3.3). The mixers behave according to specifications. With the applied filtering and amplification an output signal has been realized which can serve as input for the error detector.

5.3.2 BER measurements

After determining the spectra in the system, the real work could begin: determination of the BER curves. The BER curves have been measured for different values of the processing gain and for a number of frequency offsets.

BER versus processing gain

Figure 5.5 shows the result of the first measurements. It can be seen that there is something strange going on from $E_b/N_0 = 26 \ldots 27$. On the transition of 26 to 27 dB the settings of the cascaded variable attenuators had to be: $E_b/N_0 = 26$: -10dB/-10dB, $E_b/N_0 = 27$: -20dB/-1dB. The actual

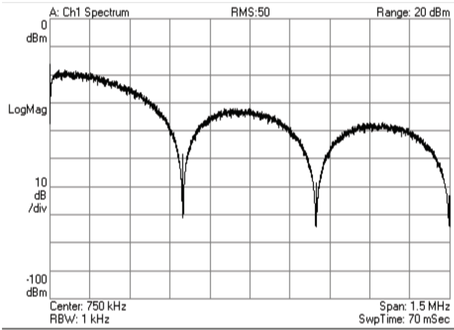

(a) Data input

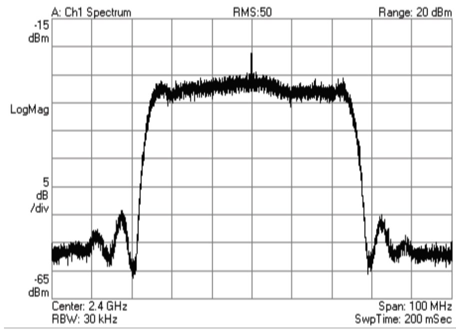

(b) Spreading sequence

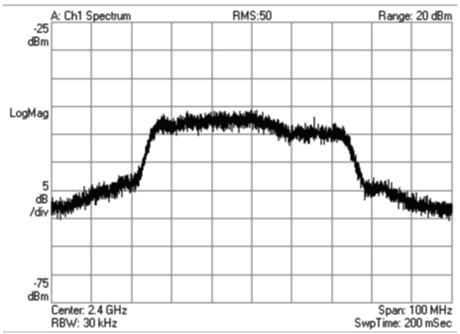

(c) Spreading sequence x Data

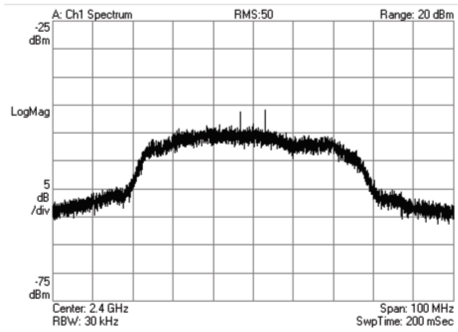

(d) Spreading sequence x Frequency offset

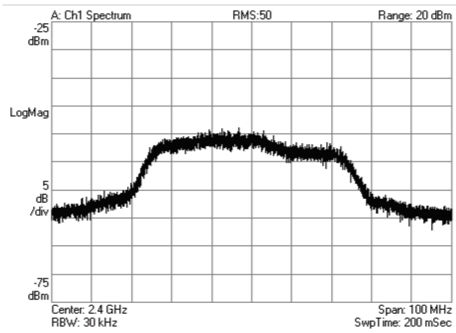

(e) Transmitter output

Figure 5.3: Spectra in the FODMA system, transmitter side

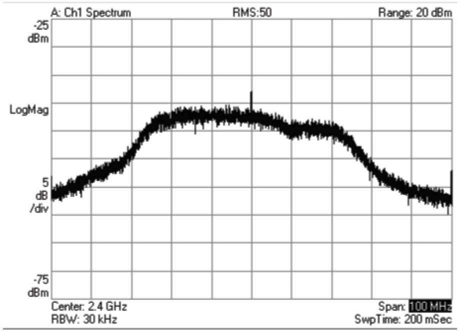

(a) Received signal x Frequency offset

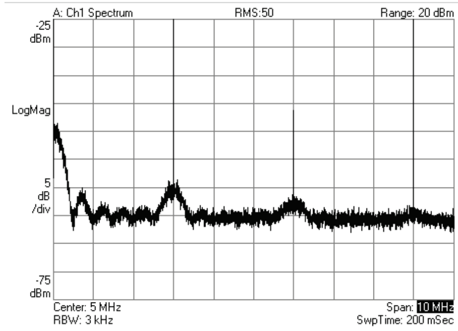

(b) Output signal, DC-10MHz

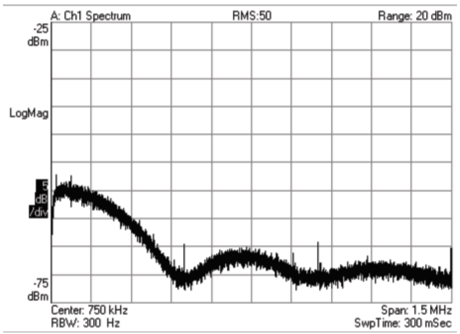

(c) Output signal, DC-1.5MHz

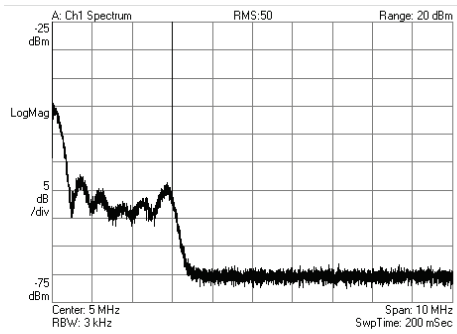

(d) Output signal, DC-10MHz, filter 1

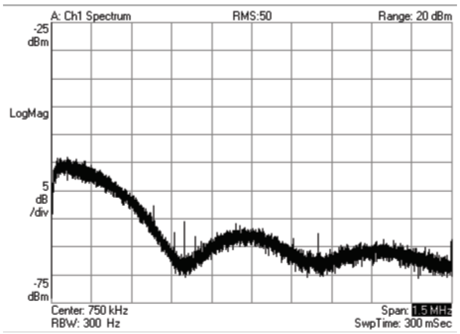

(e) Output signal, DC-1.5MHz, filter1

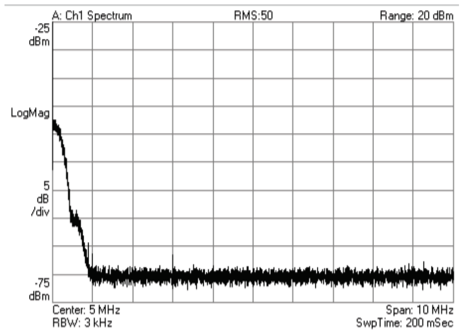

(f) Output signal, DC-10MHz, filter 2

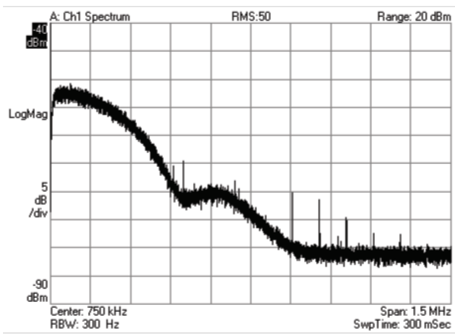

(g) Output signal, DC-1.5Mhz, filter2

Figure 5.4: Spectra in the FODMA system, receiver side

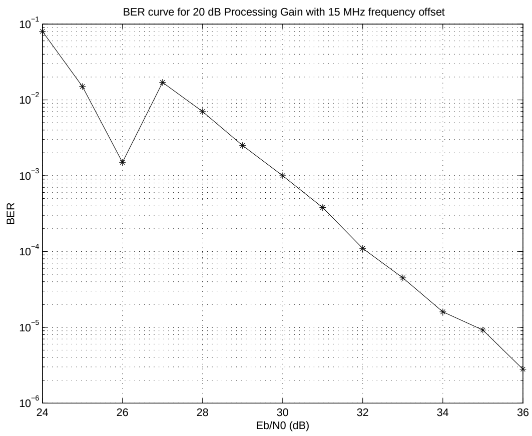

Figure 5.5: BER curve from FODMA with a 15 MHz frequency offset

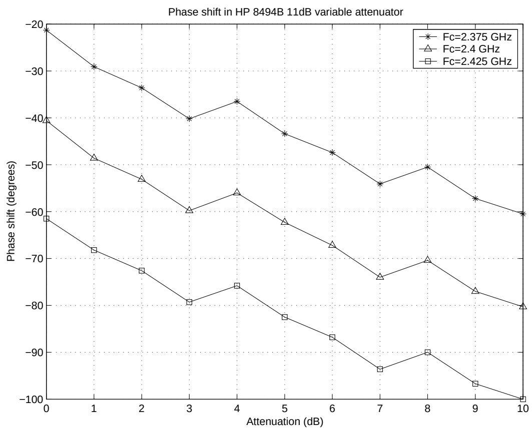

Figure 5.6: Phase shifts in the HP 8494B variable attenuator

attenuation of the attenuators has been measured using a spectrum analyzer and showed no irregular behavior. However, the phase shift in the attenuators turned out to be attenuation dependent, as can be seen from Figure 5.6. Since the noise is not real gaussian noise but a pseudo-random BPSK sequence around 2.4 GHz, this phase shift is crucial for the system performance. The output signal is, as said before a pseudo random BPSK sequence around 2.4 GHz. The constellation diagram of BPSK modulation lies entirely on the real axis of the I/Q plane. When the noise, which also is a BPSK sequence, is added to the output signal and this noise is orthogonal to the output signal, it is of no influence to the system.

To overcome the noise problem, a different noise source had to be used. Using a second vector signal generator, which could be borrowed from the

ICD/S&S group, a 50 MHz wide noise source with 4-QAM modulation has been generated. By using the QAM modulation, this channel noise occupies the entire I/Q plane and thus will not be purely orthogonal to the output signal. Also, by using this second VSG, it was not necessary to use the variable attenuators anymore, since the output power could be controlled at the VSG itself.

With this new setup, the results as shown in Figure 5.7 have been obtained. In Figure 5.7(a) the BER curves for low processing gain factors are shown. Here, the predicted error floors are clearly observed. In Figure 5.7(b) and 5.7(c) no error floors are visible. The error floors for these processing gains are so low that measurement is no longer practical.

In Figure 5.7(d) the BER curves for processing gains of 17, 20 and 23 dB obtained by measurements are given together with the analytical results (dashed) for these processing gains. It can be seen that the performance of the testbed is about 10dB worse than predicted from theory. This difference can mainly be attributed to signal losses in the components.

BER versus frequency offset

The FODMA is designed to be a multiple user system. Each user can have their own channel in the same frequency band when an unique frequency offset is assigned. This frequency offset must be in the range $B_{data} \ll \mathrm{d}f \ll B_{ss}$. Measurements have been done for offset frequencies between 3 and 15 MHz.

While doing these measurements, the output power of the system turned out to be dependent on the applied offset frequency. Also, to obtain maximum output power, the phase shift applied by the coaxial phaseshifter in the upper branch of the receiver (see Figure 5.2) had to be adjusted for each offset frequency. In Figure 5.8 the phase shift for maximum output power is plotted together with the output power in the frequency band from $0 \ldots 1$ MHz at this optimal phase shift.

Apparently, there is an IF-port frequency dependent phase shift in the mixers! Unfortunately, measurement of the phase shift in mixers as a function of IF input frequency could not be carried out.

As can be expected from Figure 5.8, the performance of the testbed is optimal at an offset frequency of 3 MHz, since the output power has a peak at that frequency. In Figure 5.9 the measurement results for frequency offsets between 3 and 15 MHz are given. In Figure 5.9(d) the BER is plotted versus the applied offset frequency at $E_b/N_0 = 36.6dB$. It can be seen that the performance of the system is highly dependent on the applied offset frequency and that performance is best at offsets of 3 and 15 MHz.

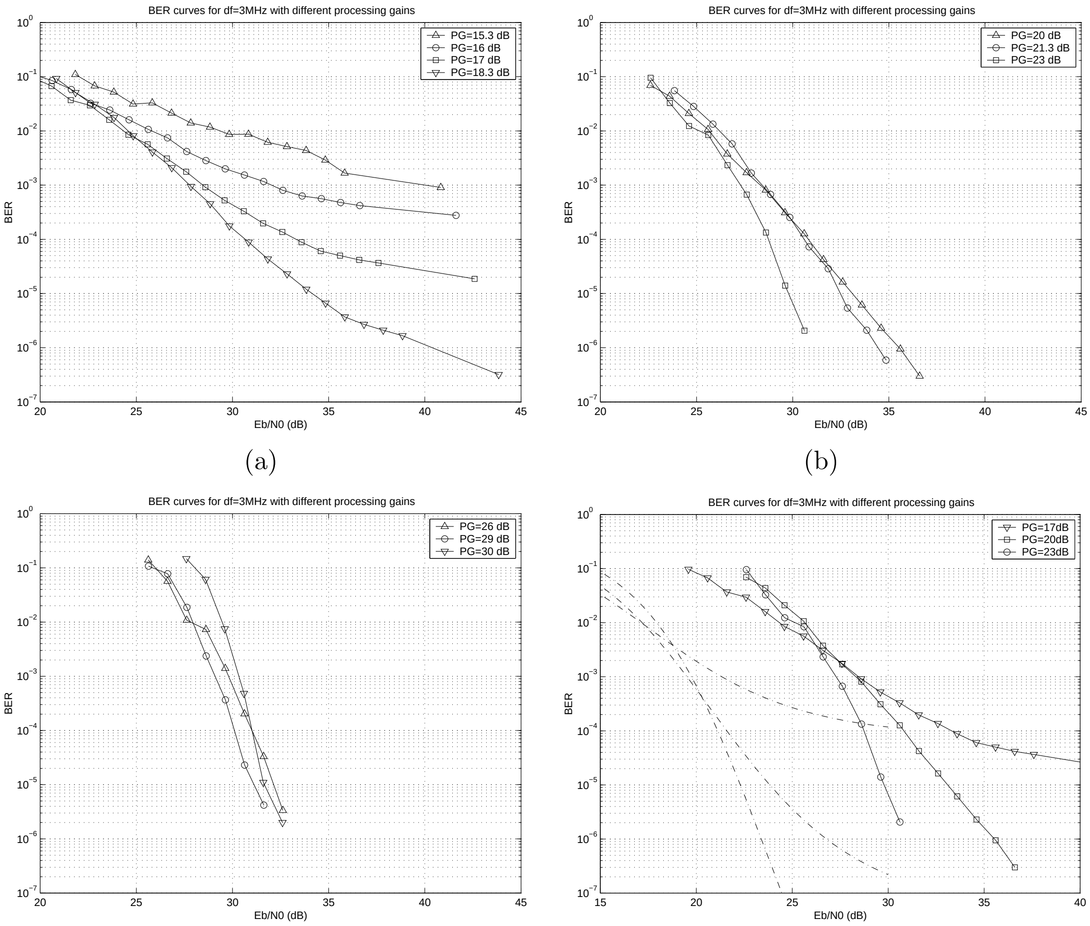

(a) (b) (c) (d)

Figure 5.7: Measurement results of BER versus Processing Gain

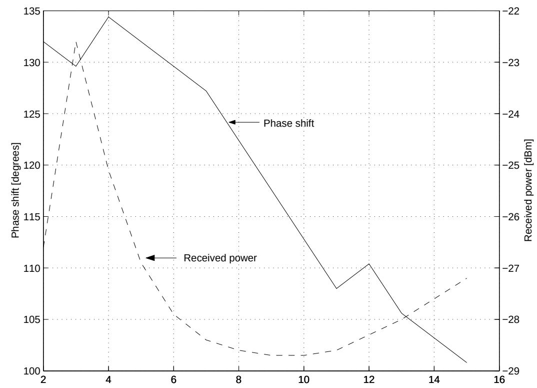

Figure 5.8: Phase shift in phase shifter for maximum output power

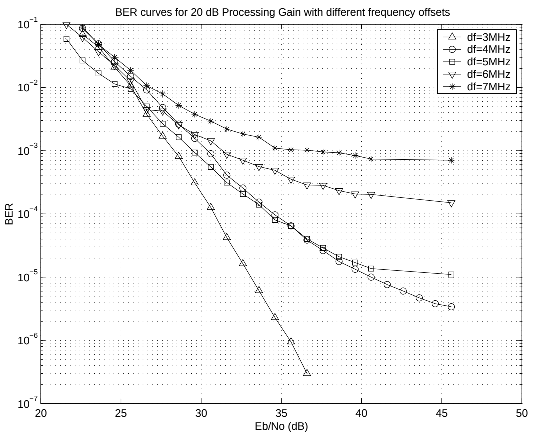

(a)

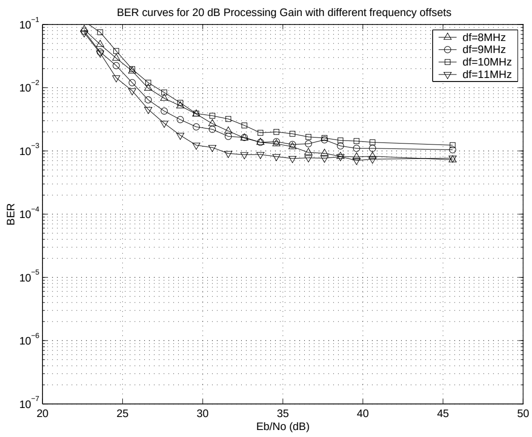

(b)

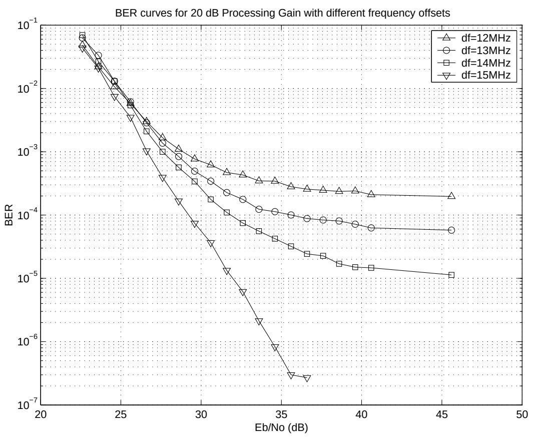

(c)

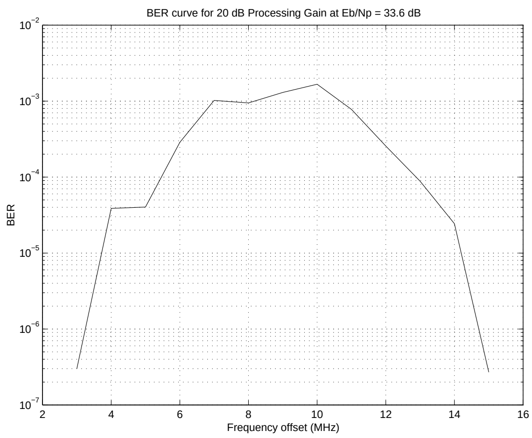

(d)

Figure 5.9: Measurement results of BER versus Frequency Offset

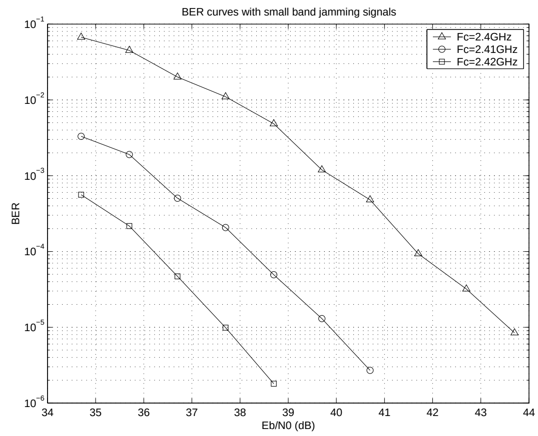

Figure 5.10: BER curves for in-band jamming signals, PG=20dB

In-band jamming

Ultra-wideband systems use an extremely high bandwidth. By despreading the signal in the receiver, the original data sequence is retrieved. As a consequence of the spreading, UWB systems are robust to small-band jamming signals. Using the second VSG, a 1 MHz wide jamming signal (QAM, pseudo random noise) has been generated. This jamming signal was varied in power and in center frequency.

In Figure 5.10 the signal output power was -12 dBm. The noise power in the 1 MHz jamming signal was varied from -16.7 to -25.7 dBm, at center frequencies of 2.4, 2.41 and 2.42 GHz. The system performance under influence of small band jammers turns out to be dependent on the position of the jamming signal. It is clear that the farther the jamming signal is from the center frequency of the spreading sequence, the better the performance.

Theoretically speaking the position of a jamming signal should not influence the system's performance. The explanation is probably associated with the generation of the spreading sequence. As mentioned before, the noise signal contains the signal's carrier frequency. This frequency is shifted in the transmitter and receiver, in the end it is present at f_c, $f_c \pm \mathrm{d}f$ and $f_c \pm 2\mathrm{d}f$. The small band jamming signal will mix back efficiently to the baseband due to these frequency terms.

5.4 Wireless operation

After successfully measuring the BER curves with a wired setup, wireless transmission has been tested using a pair of 2.4 GHz monopole antenna's.

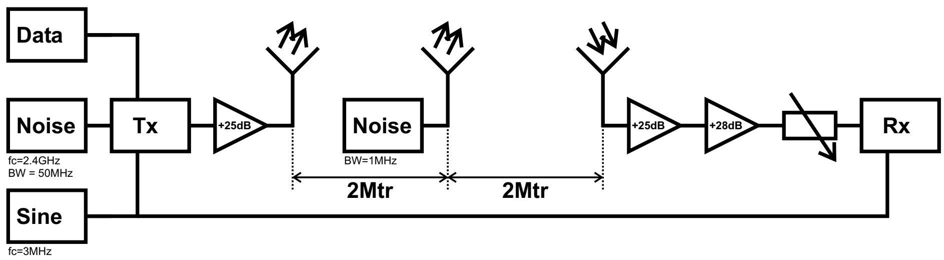

Figure 5.11: FODMA setup for wireless transmission

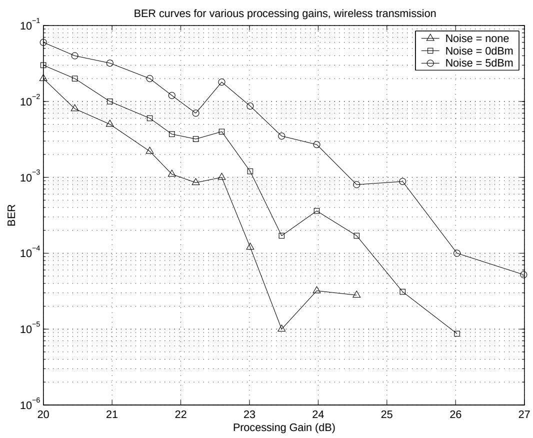

Figure 5.12: Measurement results for wireless transmission with varying processing gains

The setup as shown in Figure 5.11 was used to determine the performance in a multipath environment.

Note that since these measurements were done in an office environment, the multipath effects could not be controlled. Shifting a chair in the vicinity of the transmitter or receiver caused the received signal to change dramatically.

BER versus processing gain

In Figure 5.12 the performance of the wireless link is given as a function of the applied processing gain. The three graphs are for varying noise levels. The noise source which is located in between the sender/receiver produces a 50 MHz bandwidth QAM noise signal whose power is varied.

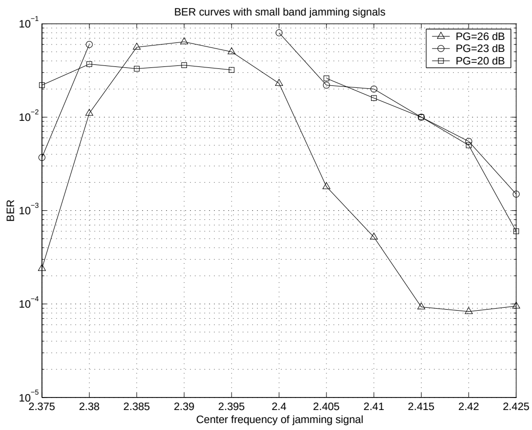

Figure 5.13: Measurement results for wireless transmission with in-band jamming

In-band jamming

In the wireless testbed, a small band jamming signal was also generated. The signal had a fixed power and was varied in frequency from 2.375 to 2.425 GHz.

In Figure 5.13 we see the same behavior as in Figure 5.10 for the wired case. It is remarkable that the performance is better when the jamming signal is at the upperside of the center frequency. A possible explanation for this phenomenon can be the matching of the antenna's. Both antenna's were a fraction longer than a quarter wavelength, resulting in optimal behavior for a frequency which is slightly lower than the desired 2.4 GHz.

Chapter 6

Conclusions and recommendations

In this report the results of the work done for simulation and realization of an FODMA testbed have been presented. The system has been simulated in ADS, using three different simulation models. The testbed has been realized with standard off-the-shelf microwave components.

6.1 Conclusions

Simulation results

The simulation parameters were set according to the system specifications of the testbed to be realized. The bandwidth of the spreading sequence was 50 MHz. By choosing bit rates from 50 Kbps to 5 Mbps the processing gain was varied from 10 to 30 dB. The simulation results (Figure 3.4 and 3.5) do not exactly match with the predictions from theory (Figure 2.6). The most important reason for this mismatch is that the simulations are a numerical approximation of the entire system, while the results from theory are purely analytical. The simulations do show the predicted behavior: error floors occur and for higher E_b/N_0 ratios, a higher processing gain gives lower bit error rates. The BER drops rapidly around an E_b/N_0 of 20 dB. This matches with the theoretical results.

Measurement results

When comparing measurements with the predictions from theory or simulation, there usually is a discrepancy between them. The most important discrepancy between the simulation results and the measured data is a difference of approximately 10 dB in performance. Where in simulation, the BER drops around $E_b/N_0 = 20$dB, in practice this drop occurs around $E_b/N_0 = 30$dB. This extremely large difference can mainly be attributed to level of detail of the simulations. Because of long simulation times, no advanced mixer model could be used when determining BER curves. The mixing losses in the real mixers are considerable. Also, LO power leakage is a major contributor to performance degradation.

The offset-frequency dependent behavior has not been explained. Probably, the mixer introduces unwanted phase shifts in the signal. As a consequence of these shifts, the 'clean' spreading signal is not in phase with the modulated signal over the entire frequency range. Since optimal despreading only occurs when the two signals arrive in phase at the correlator, the output power is drastically reduced.

The spreading sequence that is used contains a peak at its center frequency. This peak has major influence on the performance under narrowband jammers at or near the center frequency. This performance degradation can be explained by the efficient mixing of the jammers with the unmodulated sinewave.

6.2 Recommendations

The recommendations that are given here can be divided over three categories: theory, simulations and measurements. They will be presented in this order.

Theory

- A mathematical derivation has to be done on the behavior of the FODMA system under narrowband jammers. Also, the influence of a continuous wave carrier in the spreading sequence has to be investigated.

- System behavior in multipath fading channels is of major importance to wireless systems. Currently there is no knowledge on the FODMA performance in such channels. Further study is recommended.

Simulations

- More detailed component models have to be used in order to simulate the system on a higher level of detail. The primary focus should be the mixer models.

- In order to compensate for the longer simulation times, other simulation techniques, such as importance sampling, have to be investigated.
- The link between ADS and the VSG and VSA should be exploited. Complex models of individual components could be replaced by real components as a part of a simulation model.

Measurements

- The BER curves have been determined in a channel with additive QAM noise. Other noise forms should be investigated.
- For better understanding of system behavior (eg. the offset frequency dependency), a thorough study of component behavior for each component is required. Special attention should be paid to the influence of mixers on the phase of the signal.
- A spreading sequence without a peak at the center frequency should be used for comparing system behavior with the available models. It is expected that this peak has a major influence to the system behavior.
- Measurements with various bandwidths should be done in order to predict the behavior when upscaling the spreading sequence bandwidth to UWB ranges.
- Currently, there is no active synchronization on the offset frequency, while correct phase and frequency of this signal are of crucial importance to system performance. Methods for quick synchronization have to be found. Possibly, a transmitted reference signal embedded in the data signal is an option.
- The power cabling from the main switchingboard to the measurement instruments are far from optimal. A different setup is recommended to minimize interference via the power supply.

Bibliography

[1] Géza Kolumban. Theoretical noise performance of correlator-based chaotic communications schemes. *IEEE Transactions on circuits and systems-I: Fundamental Theory and Applications*, 47(12):1692–1701, December 2000.

[2] A. Meijerink. A generalization of a coherence multiplexing system. Master's thesis, University of Twente, February 2001.

[3] A. Bekkaoui. Link performance of the time offset transmitted reference system. Master's thesis, University of Twente, July 2001.

[4] A. Taban. Microwave radio testbed for a new modulation scheme based on time offset. Master's thesis, University of Twente, July 2004.

[5] Xiaoxin Shang. New radio multiple access technique based on frequency offset division multiple access (FODMA). Master's thesis, University of Twente, april 2004.

[6] Simon Haykin. *An Introduction to Analog and Digital Communications*. John Wiley & Sons, 1989.

[7] Minicircuits. ZX05-30W data sheet. http://www.minicircuits.com/cgi-bin/spec?cat=mixer&model=ZX05-30W&pix=fl905.gif&bv=4.

[8] Minicircuits. ZN2PD2-50 data sheet. http://www.minicircuits.com/cgi-bin/spec?cat=splitter&model=ZN2PD2-50&pix=vvv845_2.gif&bv=4.

[9] Minicircuits. ZRL-2400LN data sheet. http://www.minicircuits.com/ZRL-2400LN.pdf.

[10] Minicircuits. ZJL-7G data sheet. http://www.minicircuits.com/cgi-bin/spec?cat=amplifier&model=ZJL-7G&pix=bw459.gif&bv=4.

[11] Minicircuits. SLP-2.5 data sheet. http://www.minicircuits.com/dg03-198.pdf.

[12] Agilent. Spectrum analyzer measurements and noise, application note 1303.

The FODMA testbed setup

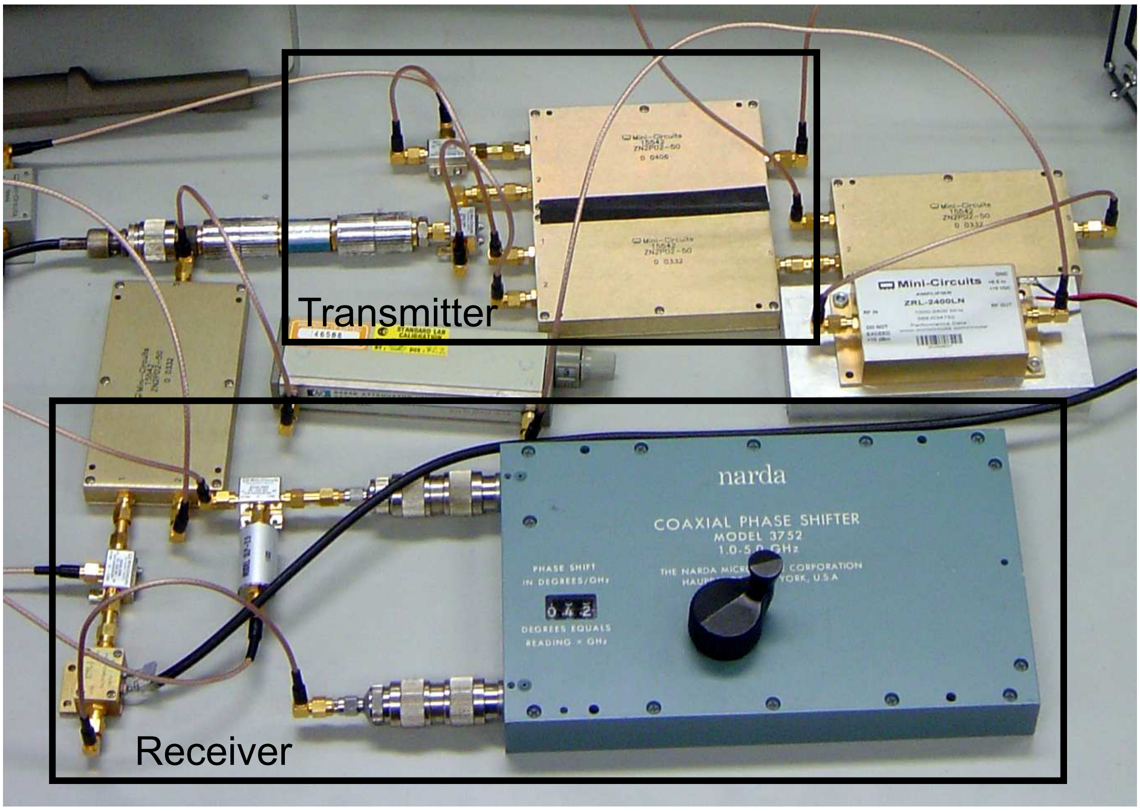

Figure 1: The FODMA transmitter and receiver

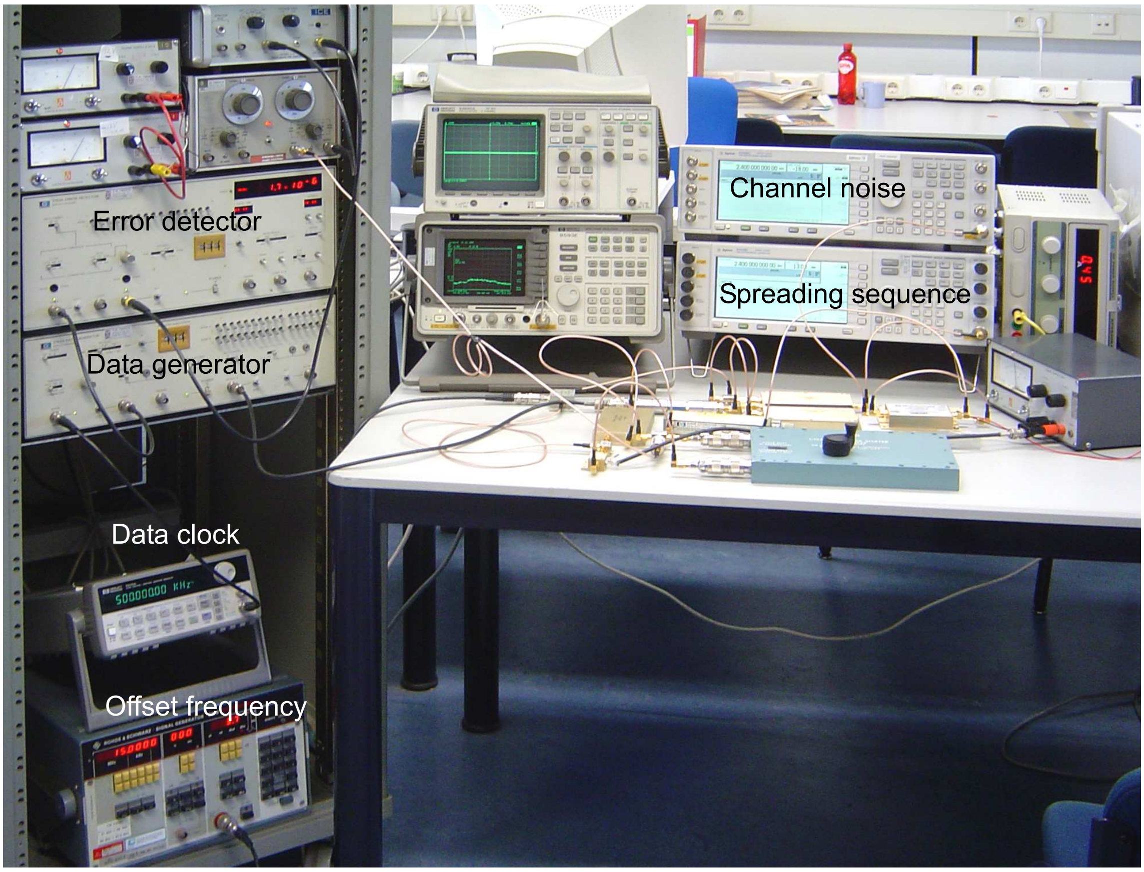

Figure 2: The entire testbed setup, wired transmission

Master assignment

Implementation of a GHz Microwave radio link applying ultra large processing gain through frequency offset.

Mobile radio communications and microwave techniques.
Prof. dr. ir. J.C. Haartsen
Prof. J.L. Tauritz

Since the first radio communication experiments carried out by Marconi around 1900, the basics of radio transceivers have hardly changed. In general, radio transceivers consist of tuned circuits with limited bandwidth. Sinusoidal waveforms are used as bearers to transport the user information. Recently, a new modulation technique has been investigated which diverges from the conventional tuned transceiver concept: **ultra-wideband** (UWB) transmission. In UWB, a very wideband transmission is used. The bandwidth is extremely large, in order of a few GHz.

UWB transceivers are attractive since they may result in very low-cost radio implementations. This is because the bearer is not based on sine waves. As a result, the radios do not contain costly filters and oscillators. The modulation method proposed for UWB by most research groups is based on ultra-short pulses. However, an alternative is to use broadband noise signals. Noise signals are easy to generate and are good candidates to serve as bearers in low-cost radio systems.

A new concept has been developed where the channel definition is not based on an *absolute* parameter but a *relative* parameter namely **frequency offset**. Basically, the concept is using spread spectrum modulation. At the transmitter, the user signal is spread with an ultra-wideband noise signal. This spread, ultra-wideband signal is then transmitted. In addition, the transmitter sends the wideband noise signal which was used for the spreading; this noise signal acts as a reference or pilot signal. To distinguish the information signal from the reference signal, a frequency offset ω_1 is applied; e.g. the reference signal is transmitted a little shifted in frequency with respect to the information signal. To retrieve the information signal, the receiver combines the information signal with the reference signal (both present in the received signal). Therefore, the receiver only has to apply the same frequency offset ω_1 and multiply the shifted signal with the originally received signal. This method allows very large spreading while fast signal acquisition is guaranteed. Thus ultra-large processing gains are feasible. We will build a demonstrator to proof concept. Recently, we acquired advanced equipment from Agilent for broadband communication measurements which are suited to implement this type of demonstrator.

The subjects of the study are:

- The design and construction of a microwave transmitter and receiver based on frequency offset modulation.
- Determining the BER performance in the presence of noise and jammers.
- Determining the processing gain.